VANÚCIA SCHUMACHER POGORZELSKI

ÍNDICES DE MONÇÃO DE VERÃO PARA O HEMISFÉRIO SUL SIMULADOS PELOS MODELOS DO CMIP

Dissertação apresentada à Universidade Federal de Viçosa, como parte das exigências do Programa de Pós-Graduação em Meteorologia Aplicada, para obtenção do título de *Magister Scientiae*.

VIÇOSA
MINAS GERAIS – BRASIL
2015

Ficha catalográfica preparada pela Seção de Catalogação e Classificação da Biblioteca Central da UFV

T

S392i
2015

Schumacher, Vanúcia, 1985-
Índices de monção de verão para o Hemisfério Sul simulados pelos modelos do CMIP / Vanúcia Schumacher. - Viçosa, MG, 2015.
vii, 70f. : il. (algumas color.) ; 29 cm.

Orientador: Flávio Barbosa Justino.
Dissertação (mestrado) - Universidade Federal de Viçosa.
Inclui bibliografia.

1. Precipitação (Metereologia). 2. Monção. 3. Hemisfério Sul. I. Universidade Federal de Viçosa. Departamento de Engenharia Agrícola. Programa de Pós-graduação em Meteorologia Aplicada. II. Título.

CDD 22. ed. 551.577

VANÚCIA SCHUMACHER POGORZELSKI

ÍNDICES DE MONÇÃO DE VERÃO PARA O HEMISFÉRIO SUL SIMULADOS PELOS MODELOS DO CMIP

Dissertação apresentada à Universidade Federal de Viçosa, como parte das exigências do Programa de Pós-Graduação em Meteorologia Aplicada, para obtenção do título de *Magister Scientiae*.

APROVADA: 17 Julho de 2015.

Marcos Paulo Santos Pereira

Paulo José Hamakawa

Flávio Barbosa Justino
(Orientador)

“Todos os caminhos são mágicos se nos levam a nossos sonhos”

Paulo Coelho

AGRADECIMENTOS

Ao meu filho Kurt, pela paciência por todos os momentos de ausência e mudanças. Ao meu marido Denison, pelo carinho e compreensão durante as horas e horas de estudo e dedicação à pesquisa.

Ao plano espiritual, pela energia e luz recebida em todos os momentos de alegria e dificuldades. À minha família, que mesmo a distância, sempre me incentivou a continuar por este caminho.

Ao meu orientador, Dr. Flávio Justino, pela dedicação e paciência; pela amizade construída e ensinamentos, e pela valiosa contribuição na realização desta pesquisa.

Aos colegas de sala Alex e Noele, pela convivência, troca de experiências e incentivo. Aos colegas Douglas, Álvaro e Marcos Paulo pela amizade e contribuição.

Aos demais colegas, professores e funcionários do Departamento de Engenharia Agrícola e da área de Meteorologia Aplicada, especialmente a Graça, pela atenção e colaboração sempre que necessário. A todos que direta e indiretamente contribuíram para essa realização.

Ao CNPq pelo apoio financeiro e a Universidade Federal de Viçosa.

SUMÁRIO

RESUMO

POGORZELSKI, Vanúcia Schumacher, M.Sc., Universidade Federal de Viçosa, julho de 2015. **Índices de monção de verão para o Hemisfério Sul simulados pelos modelos do CMIP**. Orientador: Flávio Justino.

O principal objetivo deste estudo foi avaliar a capacidade dos modelos climáticos do CMIP5 em representar a variabilidade interanual dos índices de monção de verão (IMVs) para o Hemisfério Sul (HS), e analisar a resposta dos padrões de teleconexões da Oscilação Antártica (AAO) com os IMVs e a precipitação durante o verão austral. Os índices foram calculados com base na metodologia encontrados na literatura, através da componente do vento em baixos níveis para três regiões de monção tropical no HS: América do Sul (SAM), Sul da África (SAF) e Austrália (AUS). Os resultados sugerem que as chuvas nos domínios de monção são comumente caracterizadas com anomalias de baixa pressão, associado com circulação ciclônica em baixos níveis e gradiente de Temperatura da Superfície do Mar. Além disso, observa-se um dipolo anômalo de pressão sobre América do Sul, e um efeito gangorra da anomalia de precipitação positiva (negativa) entre SAM (AUS). Nota-se também que o índice da AUS modula as chuvas em grande parte da África. As chuvas monçônicas são bem correlacionadas com a fase positiva da AAO. Em geral, os modelos CMIP5 apresentam grande variabilidade espacial entre si, e em termos de amplitude dos valores. Observa-se também que os modelos que apresentam menores contrastes de precipitação e temperatura em relação aos dados observados, reproduzem relativamente bem às simulações em comparação com o observado.

ABSTRACT

POGORZELSKI, Vanúcia Schumacher, M.Sc., Universidade Federal de Viçosa, July, 2015. **Summer monsoon indices for Southern Hemisphere simulated by CMIP models**. Adviser: Flávio Justino.

The purpose of this study is to evaluate the ability of climate models CMIP5 in representing the interannual variability of summer monsoon indices (IMVs) in Southern Hemisphere (SH), and analyze the response of teleconnections patterns of the Antarctic Oscillation (AAO) with IMVs and precipitation during the southern summer. The indices were calculated based on the methodology in the literature, through the wind component at low levels for three regions of tropical monsoon in SH: South America (SAM), South Africa (SAF) and Australia (AUS). The results suggest that rainfall in the monsoon domains are usually characterized with low pressure anomalies associated with cyclonic circulation at low levels and Sea Surface Temperature gradient. In addition, there is an anomalous dipole pressure on South America, and one seesaw effect of positive precipitation anomaly (negative) between SAM (AUS). It is noted also that the AUS index modulates the rains in much of Africa. The monsoon rains are well correlated with the positive phase of the AAO. In general, CMIP5 models have large spatial variability among themselves and in terms of amplitude values. It is also observed that the models exhibit lower contrasts precipitation and temperature in relation to the observed datasets, to reproduce relatively well the simulations compared with observed.

CAPÍTULO 1
INTRODUÇÃO GERAL

O sistema de monção global representa o modo dominante da variação anual da circulação tropical (WANG; DING, 2008), caracterizado pelo contraste sazonal da precipitação, com chuvas intensas no verão e escassez durante o inverno, associado a eventos extremos e desastres naturais (ZHISHENG et al., 2014). O regime de monção engloba várias regiões da faixa tropical do globo, impactando cerca de 70% da população que vive em países em desenvolvimento nessas regiões, influenciando diretamente a economia, onde o principal foco econômico é baseado na agricultura (GAN, 2009; ZHISHENG et al., 2014). Portanto, pesquisas que objetivem avaliar a dinâmica das monções são fundamentais, não somente pelo interesse científico, mas também para a prevenção e mitigação sócio-econômica dos seus efeitos.

A definição clássica de monção é dada pela reversão da direção dos ventos sazonalmente, entre a estação de inverno (seca) e verão (chuvosa) (MORAN; MORGAN, 1986). A variabilidade anual associada à estação chuvosa ocorre quando os ventos sopram do oceano para o continente, transportando ar quente e úmido, e a estação seca, quando os ventos revertem, trazendo ar frio e seco do interior do continente em direção ao oceano (WEBSTER et al., 1998).

Além disso, a monção é conduzida pelo ciclo sazonal de radiação solar e pelo contraste térmico entre continente-oceano, favorecendo a convecção durante a estação de verão (maior contraste térmico), também associada com a posição climatológica da Zona de Convergência Intertropical (ZCIT) (ASNANI, 1993). A forçante térmica depende da orografia e controla a intensidade e o domínio regional de monções (IPCC, 2013). Essas características marcam o início da estação chuvosa em diferentes domínios de monções como na Índia, Austrália, Ásia, África, América do Norte e Sul, sendo a região central da América do Sul (SAM), sul da África (SAF) e Austrália (AUS) parte do domínio de monções para o Hemisfério Sul (HS), foco deste estudo.

As variações no regime de precipitação de monção são moduladas por diferentes modos de variabilidade e teleconexões. O papel da Temperatura da

Superfície do Mar (TSM), do El-Niño Oscilação Sul (ENOS) e Dipolo do Oceano Índico (DOI) são importantes condutores associado às anomalias de convecção em regiões de monção (VEIGA et al., 2002; CAI et al., 2011; JOURDAIN et al., 2013; DIEPPOIS et al., 2015; HUIJUN et al., 2015; RUIQING et al., 2015), além de outras influências, como a Oscilação Decadal do Pacífico e a Oscilação Multidecadal do Atlântico (YIHUI et al., 2015). Estudos também apontam relações das chuvas de monção com a Oscilação Antártica (AAO) (XUE et al., 2004; VASCONCELLOS; CAVALCANTI, 2010; FENG et al., 2014). O papel dessas conexões com as monções são muito bem documentadas para alguns domínios de monção, como por exemplo, Austrália e Ásia, mas poucos estudos exploram as similaridades destas teleconexões entre as diferentes regiões de monção, principalmente para os domínios do HS.

As monções regionais possuem características próprias associadas às configurações topográficas e interações continente-atmosfera-oceano. Contudo, YIM et al. (2013) identificaram que as chuvas em diferentes domínios de monção são comumente caracterizadas com um padrão de circulação ciclônica em baixos níveis, em ambos os hemisférios, e forte anomalia de oeste no lado oeste-equatorial das chuvas de monção. Além disso, diversos índices de monção baseados em circulação atmosférica tem sido propostos como melhor ferramenta para identificar o início e o fim da estação chuvosa e a variabilidade das chuvas de monção, devido ao fato de a previsibilidade dos modelos climáticos em estimar as componentes de vento ser melhor que a precipitação (GAN et al., 2006; KAJIKAWA et al., 2009).

Estudos recentes têm avaliado a previsibilidade e a capacidade de simulação de diferentes Modelos de Circulação Geral (MCGs) ou simulações por conjunto (*ensemble*), associado a sistemas de monção regional ou global (KNUTTI; SEDLÁČEK, 2012; LEE; WANG, 2014; SONG; ZHOU, 2014; PARTH SARTHI et al., 2015; SHARMILA et al., 2015). Contudo, ainda há grande incerteza relacionada às simulações do clima presente e projeções futuras pelos MCGs, além de poucas pesquisas desenvolvidas considerando os domínios de monção do HS de forma integrada.

1.2 Objetivo Geral

Com base no exposto, o objetivo deste trabalho foi avaliar a representação dos índices de monção de verão no HS baseado nos modelos climáticos do Projeto de Intercomparação de Modelos Acoplados, Fase 5 (CMIP5).

1.2.1 Objetivos específicos

- Comparar o desempenho das simulações dos modelos CMIP5 para o HS com reanálises e dados observados.
- Analisar a variabilidade interanual e teleconexões entre os índices de monção de verão no HS.
- Avaliar a resposta dos índices e a precipitação de monção de verão com a Oscilação Antártica.

1.3 Estrutura da Dissertação

O presente trabalho é proposto em formato de artigo e capítulos, dividido em quatro capítulos. No capítulo 2 é apresentada a revisão de literatura. O capítulo 3 aborda os métodos numéricos e modelos climáticos. O capítulo 4 é composto pelo artigo a ser submetido na Journal of Applied Meteorology and Climatology, dividido em seções: introdução, dados e metodologia, resultados, conclusão e referências.

CAPÍTULO 2
REVISÃO DE LITERATURA

2.1 Variabilidade climática no Hemisfério Sul

Os continentes do HS possuem diferentes regimes climáticos devido sua extensão meridional, estendendo-se desde áreas equatoriais a altas latitudes, abrangendo regiões com cadeias montanhosas como a Cordilheira dos Andes na América do Sul, Drakensberg na África do Sul e pela cordilheira Australiana, configurando grandes diferenças topográficas, além da forte influência dos oceanos que cercam os continentes. Esses fatores contribuem ao desenvolvimento de diferentes sistemas atmosféricos atuantes em diferentes escalas espaciais e temporais (REBOITA et al., 2012; DEZFULI et al., 2015).

A circulação de monção representa o modo mais importante da variabilidade da precipitação na região tropical. As características e aspectos climatológicos dos sistemas de monção tem sido alvo de pesquisas em diferentes domínios: Ásia (WEBSTER et al., 1998; DING, 2007; SPERBER et al., 2013), Austrália (HOLLAND, 1986; KIM et al., 2006; SHENG-PING, 2015), América do Sul (GAN et. al, 2004; MECHOSO et al., 2005; ZAMBONI et al., 2012), África (SULTAN; JANICOT, 2003; SEGELE et al., 2015), com exceção para a região da África do Sul que tem sido pouco explorada na literatura.

As teleconexões são importantes mecanismos de variabilidade do clima, responsáveis pela ocorrência de eventos anômalos e influência na circulação atmosférica, caracterizado por diferentes padrões espaciais e temporais (CAVALCANTI; AMBRIZZI, 2009). A variabilidade interanual da precipitação em regiões tropicais é fortemente modulada pela teleconexão do fenômeno ENOS (GOSWAMI; XAVIER, 2005; YIM et al., 2013; JOURDAIN et al., 2013; DIEPPOIS et al., 2015), caracterizado pelo acoplamento oceano-atmosfera, responsável por alterações na TSM, pressão, vento e convecção tropical, sendo episódios de El Niño (La Niña) fases opostas desta oscilação, marcado pelo aquecimento (esfriamento) anômalo na região leste-central do Pacífico equatorial (GRIMM, 2009). Os efeitos do ENOS no clima do HS incluem aumento das chuvas durante a fase fria (La Niña) no sul da África e

Austrália, e o oposto sobre a região sul e central-leste da AS (HOPELEWSKI; HALPERT, 1987).

O padrão dominante da variabilidade extratropical do clima no HS é representado pela AAO, caracterizada pela anomalia de pressão entre médias e altas latitudes do HS (GONG; WANG, 1999). Thompson e Wallace (2000) identificaram estruturas anelares zonalmente simétricas, caracterizadas por perturbações de altura geopotencial de sinais opostos centrados nos pólos e em torno da latitude 45ºS, do qual chamaram de “Modo Anelar Sul”. Essas estruturas ou modos anelares ocorrem em ambos os hemisférios da circulação extratropical, o equivalente a Oscilação do Ártico no Hemisfério Norte (HN).

A fase negativa (positiva) da AAO durante o verão austral é associada com padrões de TSM, convecção e anomalias de circulação que se assemelham à fase El Niño (La Niña) do ENOS (CARVALHO et al., 2005). Além disso, padrões de teleconexões também estão associados a anomalias de precipitação em diferentes partes do globo. Xue e Wang (2004) mostraram que a variabilidade da Alta da Mascarena e a Alta da Austrália são dominadas pela AAO, intensificando as chuvas no leste da monção da Ásia. Hendon et al. (2007) notaram que a fase positiva da AAO está associada com a diminuição das chuvas sobre o sudeste e sudoeste da Austrália durante o inverno boreal, e no verão é associado com aumento da precipitação na costa leste do sul da Austrália e diminuição na Tasmânia ocidental. A fase positiva da AAO também é relacionada com extremos de chuva durante o verão no sudeste do Brasil (VASCONCELLOS; CAVALCANTI, 2010).

2.2 Regimes de Monções

Existem na literatura diferentes definições para caracterizar as regiões que se enquadram no regime de monção. O conceito tradicional, já assinalado, é associado à reversão sazonal do vento contrastando verões chuvosos e invernos secos (MORAN; MORGAN, 1986). Fisicamente, o que causa a circulação monçônica é a resposta da interação atmosfera-continente-oceano devido ao contraste térmico (TRENBERTH et al., 2000; ZHISHENG et al., 2014). Estudos baseado na definição de monção em termos das características da precipitação tem mostrado distintas regiões monçônicas em ambos os

hemisférios, no qual as diferenças entre os diferentes domínios dependem da distribuição continente-oceano, bem como gradientes de TSM e topografia. Os domínios regionais de monção durante o verão no HS (SAM, SAF e AUS) são representados na Figura 1.

A caracterização do regime de monção sobre a AS só foi realmente admitida após a identificação da reversão sazonal na direção dos ventos em baixos níveis, quando a componente média anual é removida, o que foi observada por Zhou e Lau (1998). Assim, a reversão torna-se explícita, mudando a direção dos ventos de sudeste para noroeste (verão austral), convergindo para a região central do Brasil, devido ao efeito de barreira dos Andes, satisfazendo os critérios de circulação de monção.

Além disso, Mechoso et al. (2005) relacionaram a precipitação de monção na AS associada com a ZCIT do Atlântico e a Zona de Convergência do Atlântico Sul (ZCAS), associado com o transporte de ar quente e úmido da região Amazônica através da Corrente de Jato de Baixos Níveis (CJBN) convergindo sobre a região central da AS, onde se encontra com a baixa do Chaco. Em altos níveis, a presença da Alta da Bolívia também é observada, configuração típica durante o verão (Figura 1a). Ainda, os mesmos autores definiram que as principais características do sistema de monção na AS é definido pela massa equatorial, orografia e TSM.

O regime monçônico durante o verão austral na AS é semelhante à monção de verão na Ásia (RAO; HADA, 1990), onde o ciclo de vida é caracterizado com máximos (mínimo) de precipitação durante dezembro-fevereiro (junho-agosto), englobando a região entre a Amazônia e o sudeste do Brasil (RAIA; CAVALCANTI, 2008).

Na África, a circulação de monção influencia o regime de chuvas no oeste da África e região sul, embora, pouca atenção e estudos têm sido realizados sobre essa região. No oeste, o padrão de circulação de monção é dado pela reversão sazonal dos ventos de sudoeste (úmido e frio) durante verão boreal para sudeste (quente e seco) no inverno boreal. A região monçônica no sul da África é associada com anomalias de precipitação ao norte de Madagascar, parte sudoeste do oceano Índico e entre a Tanzânia-Moçambique, além disso, anomalia ciclônica em baixos níveis centrada em Madagascar (YIM et al., 2013).

A monção da Austrália engloba uma das componentes do sistema de monções Ásia-Austrália, sendo influenciada pela variabilidade climática tropical e subtropical (KAJIKAWA et al., 2009), ou seja, o máximo de aquecimento associado ao período chuvoso ocorre durante o verão boreal na Ásia convergindo para o continente marítimo (região entre o continente Asiático e Austrália) e norte da Austrália. O regime de circulação de monção de verão na Austrália é caracterizado pela reversão da anomalia dos ventos em baixos níveis, de leste para oeste, sobre a região norte acompanhado do aumento de precipitação (KIM et al., 2006). O forte gradiente de temperatura entre o continente asiático e região da Indonésia fortalece os ventos equatoriais.

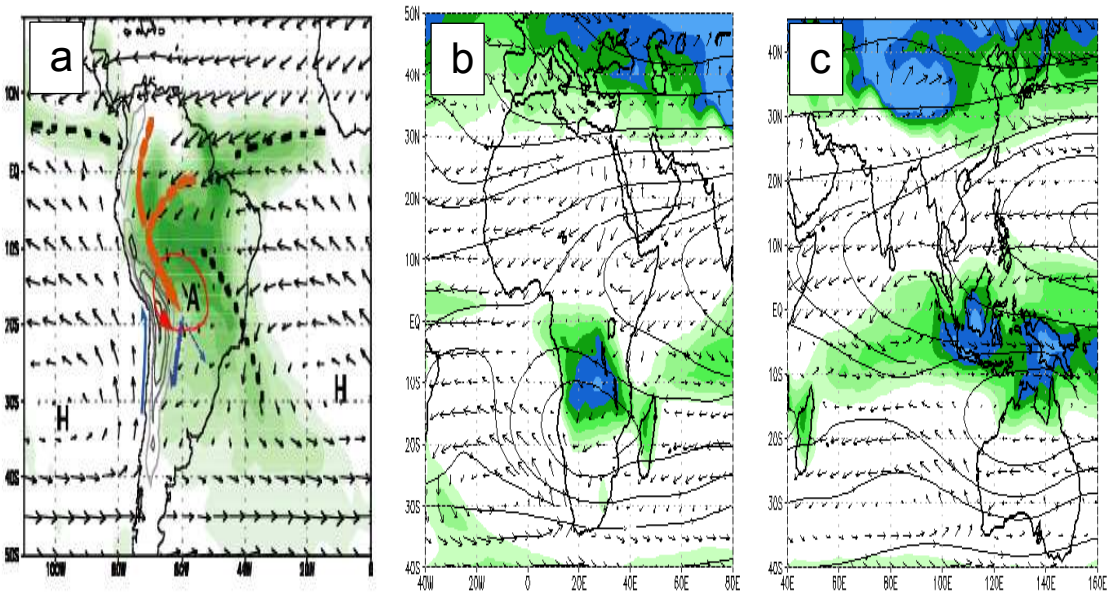

Figura 1- Esquema ilustrativo do sistema de monção na América do Sul (a), África do Sul (b) e Austrália (c). Em (a) a parte sombreada é referente à precipitação e as linhas tracejadas a ZCIT e a ZCAS. Os vetores menores indicam o vento em baixos níveis (900 hPa), vetores maiores estão associados a CJBN, H indica o Anticiclone Subtropical e A a Alta da Bolívia. Em (b) e (c) a parte sombreada é referente à radiação de onda longa (Wm^{-2}), linhas de corrente em 200 hPa e vetor ventos zonal em 850 hPa. Fonte: Mechoso et al. (2005) (a), http://www.cpc.ncep.noaa.gov (b-c).

2.3 Influencia das mudanças climáticas nas monções

As projeções climáticas para os diferentes domínios de monções apresentadas no Painel Intergovernamental de Mudanças Climáticas (do acrônimo em inglês, IPCC/AR5) indicam um aumento (enfraquecimento) nas chuvas (circulação) de monção. A variabilidade do regime de monção é influenciada por diferentes fatores e forçantes relacionado com os efeitos das mudanças climáticas que afetam o contraste térmico entre oceano-continente, cobertura e uso do solo, conteúdo de água na atmosfera, concentração de aerossóis, entre outros (IPCC, 2013; YIHUI et al., 2015). As projeções associadas à variação desses fatores na perspectiva das alterações climáticas são mostrados na figura 2, e discutidos abaixo:

(i) As mudanças no uso do solo alteram o albedo da superfície, alterando o aquecimento no continente;

(ii) Além disso, o aumento da quantidade de aerossóis contribui para o aquecimento da atmosfera devido à absorção de radiação solar pelos aerossóis, que por outro lado, também afeta a quantidade de radiação que atinge a superfície, podendo alterar a circulação de monção associado à alteração da distribuição de aquecimento da superfície terrestre. As forçantes positiva e negativa dos aerossóis contribuem na desestabilização da atmosfera, determinando os gradientes de pressão horizontal que modulam a circulação e precipitação de monção (YIHUI et. al, 2015).

(iii) O aquecimento da atmosfera resulta em um *feedback* positivo, aumentando a quantidade de umidade atmosférica e contribuindo para o aumento no total das chuvas de monções, mesmo que a circulação de monção enfraqueça ou não altere.

Apesar das incertezas associadas às tendências no futuro das monções projetado pelos MCGs, diversos estudos apresentados no último IPCC tem mostrado o aumento na intensidade e no total da precipitação de monção global, associado ao aumento da convergência de umidade e evaporação em superfície devido ao enfraquecimento da circulação de monção (IPCC, 2013; KITOH et al., 2013).

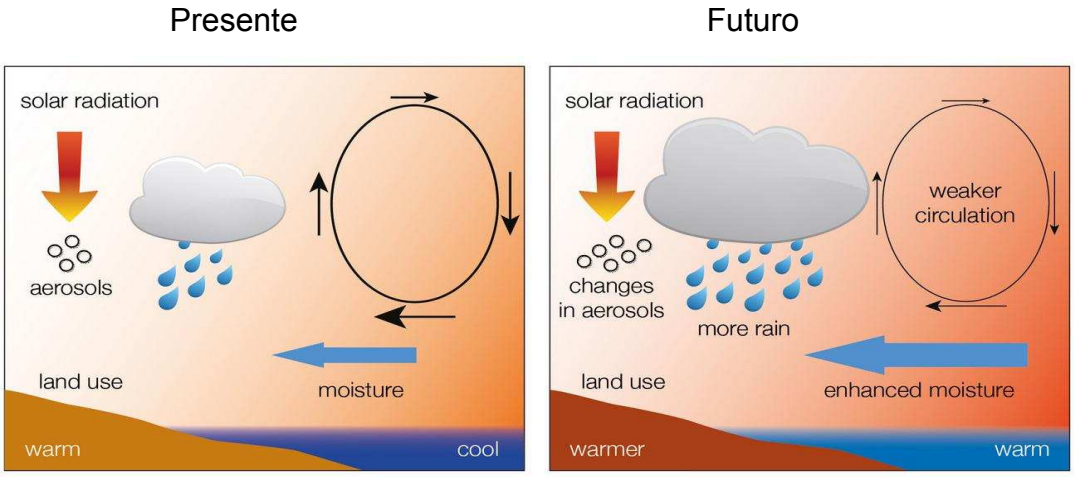

Figura 2- Esquema da influência das mudanças climáticas nas chuvas de monção. Fonte: IPCC (2013).

Baseado no cenário intermediário de mudanças climáticas, o aumento médio da precipitação global previsto é de 3,2%K^{-1} segundo Hsu et al. (2013). Por outro lado, o aumento esperado para monção de verão na Índia é de 5%/ºC, 6,4%/ºC no leste da Ásia e 2,6%/ºC para Austrália (WANG et al., 2014). Além disso, um aumento da precipitação sobre a África do Sul e norte–sudeste da Austrália seria esperado durante o verão austral (2070-2095) (LEE; WANG, 2014). O Aumento no total da precipitação monçônica sobre a América do Sul também seria observada, principalmente sobre o sul do Brasil, Uruguai e norte da Argentina (JONES; CARVALHO, 2013).

CAPÍTULO 3
MODELOS CLIMÁTICOS E MÉTODOS NUMÉRICOS

3.1 Modelos Climáticos do CMIP

O Projeto de Intercomparação de Modelos Acoplados, Fase 5 (*Coupled Model Intercomparison Project* - CMIP5) compreende o novo conjunto de experimentos de modelos climáticos proposto em 2008, envolvendo grupos de modelagem de diferentes países, *World Climate Research Programme's* (WCRP), *Working Group on Coupled Modelling* (WGCM), *International Geosphere–Biosphere Programme's* (IGBP) e *Analysis, Integration and Modeling of the Earth System* (AIMES), visando um conjunto de simulações climáticas que se concentram na compreensão do passado e futuras mudanças climáticas, do qual as análises dos resultados foram apresentados no Quinto Relatório de Avaliação do Painel Intergovernamental sobre Mudanças Climáticas (AR5/IPCC). O CMIP5 tem a finalidade de: i) avaliar os mecanismos responsáveis pelas diferenças dos modelos e *feedbacks* associados ao ciclo de carbono e nuvens; ii) a "previsibilidade" do clima e explorar a capacidade de sistemas de previsão em escalas de tempo decadal; e iii) determinar os fatores que induzem modelos com forçantes similares produzirem uma variedade de respostas diferentes (TAYLOR et al., 2009).

O CMIP5 apresenta dois tipos de experimentos associados a mudanças climáticas, longo prazo (historical) e curto prazo (experimento decadal de previsão, 10-30 anos) adicionado no CMIP5, sendo inicializado com condições de gelo e oceano. A habilidade de previsão de curto prazo depende da habilidade dos modelos, da qualidade e cobertura das observações do oceano (TAYLOR et al., 2012). O conjunto de projeções futuras (*representative concentration pathways*-RCPs) é dividido em cenários de emissões, baseado em projeções de crescimento populacional e forçantes radiativas, descritos em Moss et al. (2010).

As principais diferenças entre o CMIP3 e o CMIP5 é a inclusão de modelos com amplo conjunto de experimentos, com melhor resolução espacial, amplo armazenamento de conjuntos de saída, documentação mais detalhada, com uma gama muito maior de novas variáveis oceânicas e atmosféricas, além

da inclusão de ciclos biogeoquímicos e novas forçantes (TAYLOR et al., 2012a).

O avanço de novos estudos e pesquisas para compreender o complexo sistema climático envolvendo o conjunto de interações acopladas entre continente, atmosfera, oceano e criosfera e seus processos físicos e dinâmicos é de extrema importância à aplicação de dados climáticos que representem esses mecanismos.

Os MCGs aplicados neste estudo fazem parte do CMIP5, obtidos no site http://pcmdi9.llnl.gov/. A seleção dos modelos foi baseada nos critérios: tipo de experimento, ensemble e série temporal, sendo escolhido apenas um modelo referente a cada centro de modelagem. Os modelos selecionados fazem parte do experimento decadal, abrangendo o período de 1981 a 2010. A descrição e referências para cada um destes modelos são dadas na Tabela 1.

Tabela 1- Descrição dos modelos CMIP5.

Modelos	Centro de Modelagem	País	MCGs resolução	Referências
BCC-CSM1.1	BCC	China	2.8º x 2.8º	(Xin et al. 2013)
CanCM4	CCCma	Canada	2.8º x 2.8º	(CHYLEK et al., 2011)
CFSv2-2011	COLA and NCEP	USA	1º x 1º	(SAHA et al., 2013)
CMCC	CMCC	Itália	2º x 2º	(SCOCCIMARRO et al., 2011)
GEOS-5	NASA GMAO	USA	2º x 2.5º	(Rienecker et al. 2008)
GFDL-CM2.1	NOAA GFDL	USA	2º x 2.5º	(DELWORTH et al., 2006)
IPSL-CM5A-LR	IPSL	França	1.9º x 3.7º	(DUFRESNE et al., 2013)
MIROC5	MIROC	Japão	1.5º x 1.5º	(WATANABE et al., 2010)
MPI-ESM-LR	MPI-M	Alemanhã	1.8º x 1.8º	(RADDATZ et al., 2007)
MRI-CGCM3	MRI	Japão	1.8º x 2.8º	(YUKIMOTO et al., 2011)

Os experimentos do CMIP5 são denominados pelo conjunto de caracteres “rxiypz” codificando as configurações das simulações. O “r” representa o número de realizações ou rodadas, “i” as diferentes inicializações com implicações físicas e o “p” são as perturbações na física para cada um dos modelos simulados. Neste trabalho foi considerado apenas um conjunto de

ensemble (r1i1p1), ou seja, rodada 1, com inicialização 1 e física 1 de cada modelo.

3.2 Reanálise e dados observados

Dados de reanálises e observados (sensoriamento remoto) também foram utilizados para validar as simulações geradas pelos modelos climáticos (1981-2010):

(i) CFSR-NCEP *(The Climate Forecast System Reanalysis - National Centers for Environmental Prediction*) (SAHA et al., 2010), versão aprimorada das reanálises 1 e 2, com resolução espacial horizontal de 0,5º de latitude e longitude, disponível em http://cfs.ncep.noaa.gov/cfsr/.

(ii) GPCP (Global Precipitation Climatology Project) (ADLER et al., 2003), combina dados de estações pluviométricas e sensoriamento remoto, com resolução 2,5º x 2,5º de latitude e longitude, obtidos: http:www.esrl.noaa.gov/psd/.

(iii) HadISST (Hadley Centre Sea Ice and Sea Surface Temperature) (RAYNER et al., 2003) resolução de 1º de latitude e longitude, disponível em http://www.metoffice.gov.uk/hadobs/hadisst/.

As variáveis médias mensais utilizadas foram: Temperatura da Superfície (TS), Temperatura da Superfície do Mar (TSM), precipitação (PR), altura geopotencial em 500 hPa (ZG), pressão a nível médio do mar (SLP), componentes do vento zonal (U) e meridional (V).

3.3 MÉTODOS NUMÉRICOS

3.3.1 Simulações dos Modelos x Reanálises

Para a comparação entre os modelos climáticos CMIP5 e as reanálises foi realizado um ajuste nas simulações através da interpolação bilinear, alterando a resolução espacial para 2° de latitude e longitude, para ambos os dados (modelos e reanálises).

A capacidade de simulação dos modelos climáticos CMIP5 foi avaliada através da diferença entre as variáveis definidas com as saídas dos modelos e reanálises, sobre o Hemisfério Sul. A significância estatística das diferenças foi calculada pelo teste t, e para precipitação o teste não paramétrico de Wilcoxon-Mann-Whitney (WILKS, 2006), com intervalo de confiança de 95%.

3.3.2 Analise Harmônica

A variabilidade espacial sazonal do comportamento das variáveis para cada modelo do CMIP5 foi descrita através do método de análise harmônica, baseada na série de funções trigonométricas (WILKS, 2006), como descrita abaixo:

$$y_t = \bar{y} + \sum_{j=1}^{N} C_j \cos\left(\omega_j t - \varphi_j\right) \qquad \text{Equação 1}$$

onde y_t é o valor no tempo t, $\bar{y}$ a média, C_j é amplitude dos harmônicos, ω_j representa a frequência, φ_j é o ângulo de fase, e N o número de observações. A amplitude é dada por:

$$C_j = \sqrt{A_j^2 + B_j^2} \qquad \text{Equação 2}$$

Sendo A_j e B_j:

$$A_j = \frac{2}{N}\sum_{t=1}^{N} y_t \cos\left(\frac{2\pi t}{N}\right) \qquad \text{Equação 3}$$

$$B_j = \frac{2}{N}\sum_{t=1}^{N} y_t \operatorname{sen}\left(\frac{2\pi t}{N}\right) \qquad \text{Equação 4}$$

O ângulo de fase é dependente de A_j, calculado como:

$$\varphi_j = \begin{cases} tan^{-1}\frac{B_j}{A_j} A_j > 0 \\ \tan^{-1}\frac{B_j}{A_j} \pm \pi \; ou \; 180º \; A_j < 0 \\ \frac{\pi}{2} \; ou \; 90º \; A_j = 0 \end{cases}$$ Equação 5

A contribuição dos harmônicos individuais j para o total de variância da serie temporal é dada por $j = \frac{C_j^2}{2s^2}$, onde s é serie temporal da variância. O primeiro harmônico mostra as características a longo prazo, enquanto que o segundo harmônico os efeitos em curto prazo.

3.3.3 Índices de monção de verão

Os índices de monção de verão (IMVs) foram calculados para os três modos dominantes no HS: SAM, SAF e AUS, computados para todos os modelos selecionados.

Os IMVs são definidos como: índice zonal e meridional (*zonal and meridional index* – UVI) para o domínio da monção na América do Sul, dado pela soma do vento zonal e meridional no nível de 850 hPa (GAN et al., 2006).

UVI = U_850(10ºS-15ºS, 60ºW-50ºW) + V_850(20ºS-25ºS, 65ºW-60ºW) Equação 6

O índice da monção de verão da África do Sul (Southern African summer monsoon index - SAFI) é definido pela diferença do vento zonal em 850 hPa (YIM et al., 2013).

SAFI = U_850(5ºS-15ºS, 20ºE-50ºE) - U_850(20ºS-30ºS, 30ºE-55ºE) Equação 7

O índice de monção da Austrália (Australian monsoon index – AUSMI) é calculado como a média zonal do vento em 850 hPa (KAJIKAWA et al., 2009).

AUSMI = U_850(5ºS-15ºS, 110ºE-130ºE) Equação 8

Para confirmar a capacidade dos índices em descrever a variabilidade interanual das monções, correlações com anomalia média sazonal da precipitação, pressão a nível médio do mar e TSM foram calculadas usando verão austral (Dezembro-Fevereiro- DJF), com 95% de confiança.

3.3.4 Funções Ortogonais Empíricas- Oscilação Antártica

Para identificar o principal padrão de teleconexão no HS - Oscilação Antártica, foi aplicada o método de Função Ortogonal Empírica (*Empirical Orthogonal Function* - EOF) (WILKS, 2006). O principal padrão da AAO é definido pelo primeiro modo da EOF.

O cálculo da AAO foi obtido por meio de campos médios mensais de anomalia da altura geopotencial em 500 hPa , entre as latitudes 20ºS a 90ºS, sendo removido o ciclo sazonal, e ponderando os dados de grade pela raiz quadrada do cosseno da latitude, para garantir a ponderação de área igual na matriz de covariância. Essa metodologia é similar ao cálculo do índice da AAO utilizado pelo Climate Prediction Center (CPC/NOAA).

3.3.4.1 Resposta da Oscilação Antártica

Para analisar a influência da AAO nas chuvas de monção no HS foi aplicado o método de compósites ou médias ponderadas, conforme segue a equação 9 .

$$\bar{x}_p = \frac{\sum_{j=1}^{k} xifi}{\sum_{j=1}^{k} fi} \qquad \text{Equação 9}$$

Sendo xi os valores da variável e fi os valores do índice (positivo ou negativo). O numerador responde a soma do produto entre a precipitação e o índice da AAO, e o denominador pela soma dos valores do índice.

Para a ponderação, o índice da AAO foi separado em positivo e negativo sobre a variável e definido pela diferença entre as duas ponderações, permitindo a identificação da variabilidade da teleconexão sobre a variável em questão regionalmente (SANTOS; FRANCO, 2011; CAMPOS, 2013).

REFERÊNCIAS

ADLER, R. F.; HUFFMAN, G. J.; CHANG, A.; et al. The Version-2 Global Precipitation Climatology Project (GPCP) Monthly Precipitation Analysis (1979–Present). **Journal of Hydrometeorology**, v. 4, n. 6, p. 1147–1167, 2003.

ASNANI. G. C. Tropical meteorology. Pune, Índia: Nobel Printers, 1993.

CAI, W.; RENSCH, P. VAN; COWAN, T.; HENDON, H. H. Teleconnection pathways of ENSO and the IOD and the mechanisms for impacts on Australian rainfall. **Journal of Climate**, v. 24, n. 15, p. 3910–3923, 2011.

CAMPOS, T. L. O. B. Influência dos padrões de variabilidade de baixa frequência na precipitação da amazônia. **Dissertação de Mestrado**, 2013.

CARVALHO, L. M. V; JONES, C.; AMBRIZZI, T. Opposite phases of the Antarctic oscillation and relationships with intraseasonal to interannual activity in the tropics during the austral summer. **Journal of Climate**, v. 18, n. 1999, p. 702–718, 2005.

CAVALCANTI, I. F. A., AMBRIZZI, T. Teleconexões e suas influências no Brasil. In: CAVALCANTI et al. (Org.). **Tempo e Clima no Brasil**. São Paulo: Oficina de Textos, 2009. cap.20, p.317-335.

CAVALCANTI, I. F. A.; CARRIL, A. F.; PENALBA, O. C.; et al. Precipitation extremes over La Plata Basin – Review and new results from observations and climate simulations. **Journal of Hydrology**, v. 523, p. 211–230, 2015. Elsevier B.V. Disponível em: <http://linkinghub.elsevier.com/retrieve/pii/S0022169415000451>. .

CHYLEK, P.; LI, J.; DUBEY, M. K.; WANG, M.; LESINS, G. Observed and model simulated 20th century Arctic temperature variability: Canadian Earth System Model CanESM2. **Atmospheric Chemistry and Physics Discussions**, v. 11, p. 22893–22907, 2011.

DELWORTH, T. L.; BROCCOLI, A. J.; ROSATI, A.; et al. GFDL's CM2 global coupled climate models. Part I: Formulation and simulation characteristics. **Journal of Climate**, v. 19, p. 643–674, 2006.

DEZFULI, A. K.; ZAITCHIK, B. F.; GNANADESIKAN, A. Regional Atmospheric Circulation and Rainfall Variability in South Equatorial Africa. **American Meteorology Society**, v. 28, p. 809–818, 2015.

DIEPPOIS, B.; ROUAULT, M.; NEW, M. The impact of ENSO on Southern African rainfall in CMIP5 ocean atmosphere coupled climate models. **Climate Dynamics**, 2015.

DING, Y. The variability of the Asian summer monsoon. **Journal of the Meteorological Society of Japan**, v. 85B, p. 21–54, 2007.

DUFRESNE, J. L.; FOUJOLS, M. A.; DENVIL, S.; et al. Climate change projections using the IPSL-CM5 Earth System Model: from CMIP3 to CMIP5. **Climate Dynamics**, v. 40, p. 2123–2165, 2013.

FENG, X.; DAN, S.; TIAN-JUN, Z. Interdecadal and Interannnual Variabilities of the Antarctic Oscillation Simulated by CAM3. **Atmosphere and Oceanic Science Letters**, v. 7, p. 515–520, 2014.

GAN, M. A.; KOUSKY, V. E.; ROPELEWSKI, C. F. The South America Monsoon circulation and its relationship to rainfall over west-central Brazil. **Journal of Climate**, v. 17, n. 1, p. 47–66, 2004.

GAN, M. A.; RAO, V. B.; MOSCATI, M. C. L. South American monsoon indices. **Atmospheric Science Letters**, v. 223, p. 219–223, 2006.

GAN, M. A.; RODRIGUES, L. R.; RAO, V. B. Monção na América do sul. In: CAVALCANTI et al. (Org.). **Tempo e Clima no Brasil**. São Paulo: Oficina de Textos, 2009. cap.19, p.297-316.

GONG, D.; WANG, S. Definition of Antarctic Oscillation index. **Geophysical Research Letters**, v. 26, n. 4, p. 459, 1999.

GOSWAMI, B. N.; XAVIER, P. K. ENSO control on the south Asian monsoon through the length of the rainy season. **Geophysical Research Letters**, v. 32, n. 18, p. 1–4, 2005.

GRIMM, A. M. Variabilidade interanual do clima no Brasil. In: CAVALCANTI et al. (Org.). **Tempo e Clima no Brasil**. São Paulo: Oficina de Textos, 2009. cap.22, p.353-374.

HENDON, H. H.; LIEBMANN, B. A composite study of onset of the Australian summer monsoon. , 1990.

HENDON, H. H.; THOMPSON, D. W. J.; WHEELER, M. C. Australian rainfall and surface temperature variations associated with the Southern Hemisphere annular mode. **Journal of Climate**, v. 20, n. 11, p. 2452–2467, 2007.

HIROKAZU, E.; AKIO, K. Thermodynamic and dynamic effects on regional monsoon rainfall changes in a warmer climate. **Geophysical Research Letters**, v. 41, n. October 2013, p. 1704–1710, 2014.

HIROTA, N.; TAKAYABU, Y. N. Reproducibility of precipitation distribution over the tropical oceans in CMIP5 multi-climate models compared to CMIP3. **Climate Dynamics**, v. 41, n. 11-12, p. 2909–2920, 2013.

HOLLAND, G. J. Interannual Variability of the Australian Summer Monsoon at Darwin: 1952–82. **Monthly Weather Review**, 1986.

HSU, P. C.; LI, T.; MURAKAMI, H.; KITOH, A. Future change of the global monsoon revealed from 19 CMIP5 models. **Journal of Geophysical Research: Atmospheres**, v. 118, n. 3, p. 1247–1260, 2013.

HUIJUN, W.; KE, F. A. N.; JIANQI, S. U. N.; et al. A Review of Seasonal Climate Prediction Research in China. , v. 32, n. February, p. 149–168, 2015.

JAKUBAUSKAS, M. E.; LEGATES, D. R.; KASTENS, J. H. Harmonic analysis of time - series AVHRR NDVI data. **Photogrammetric engineering and remote sensinghotogrammetric engineering and remote sensing**, v. 67, n. 4, p. 461 – 470, 2001.

JOURDAIN, N. C.; GUPTA, A. SEN; TASCHETTO, A. S.; et al. The Indo-Australian monsoon and its relationship to ENSO and IOD in reanalysis data and the CMIP3/CMIP5 simulations. **Climate Dynamics**, v. 41, n. 11-12, p. 3073–3102, 2013.

JUSTINO, F.; PELTIER, W. R. Climate anomalies induced by the Arctic and Antarctic Oscillations: Glacial Maximum and present-day perspective. **Journal of Climate**, v. 21, p. 459–475, 2008.

JUSTINO, F.; SETZER, A.; BRACEGIRDLE, T. J.; et al. Harmonic analysis of climatological temperature over Antarctica: Present day and greenhouse warming perspectives. **International Journal of Climatology**, v. 31, p. 514–530, 2011.

KAJIKAWA, Y.; WANGA, B.; YANG, J. A multi-time scale Australian monsoon index. **International Journal of Climatology**, v. 1, 2009.

KIM, K. Y.; KULLGREN, K.; LIM, G. H.; BOO, K. O.; KIM, B. M. Physical mechanisms of the Australian summer monsoon: 2. Variability of strength and onset and termination times. **Journal of Geophysical Research: Atmospheres**, v. 111, n. 20, 2006.

KITOH, A.; ENDO, H.; KRISHNA KUMAR, K.; et al. Monsoons in a changing world: A regional perspective in a global context. **Journal of Geophysical Research: Atmospheres**, v. 118, n. 8, p. 3053–3065, 2013.

KNUTTI, R.; SEDLÁČEK, J. Robustness and uncertainties in the new CMIP5 climate model projections. **Nature Climate Change**, , n. October, p. 1–5, 2012.

KULLGREN, K.; KIM, K. Y. Physical mechanisms of the Australian summer monsoon: 1. Seasonal cycle. **Journal of Geophysical Research: Atmospheres**, v. 111, n. 20, p. 1–13, 2006.

LEE, J. Y.; WANG, B. Future change of global monsoon in the CMIP5. **Climate Dynamics**, v. 42, n. 1-2, p. 101–119, 2014.

MARENGO, J. A.; LIEBMANN, B.; GRIMM, A. M.; et al. Recent developments on the South American monsoon system. **International Journal of Climatology**, v. 32, n. 1, p. 1–21, 2012.

MECHOSO, C. R. Relationships between upper level circulation over South America: a physical base for seasonal predictions. .

MECHOSO, C. R.; ROBERTSON, A. W.; ROPELEWSKI, C. F.; GRIMM, A. M. The American Monsoon Systems. **The Global Monsoon System: Research and Forecast. WMO – IWM-III**, v. 13, p. 197–206, 2005.

MOSS, R. H.; EDMONDS, J. A; HIBBARD, K. A; et al. The next generation of scenarios for climate change research and assessment. **Nature**, v. 463, p. 747–756, 2010.

NIETO-FERREIRA, R.; RICKENBACH, T. M. Regionality of monsoon onset in South America: A three-stage conceptual model. **International Journal of Climatology**, v. 31, n. 9, p. 1309–1321, 2011.

PARTH SARTHI, P.; GHOSH, S.; KUMAR, P. Possible future projection of Indian Summer Monsoon Rainfall (ISMR) with the evaluation of model performance in Coupled Model Inter-comparison Project Phase 5 (CMIP5). **Global and Planetary Change**, v. 129, p. 92–106, 2015.

RADDATZ, T. J.; REICK, C. H.; KNORR, W.; et al. Will the tropical land biosphere dominate the climate-carbon cycle feedback during the twenty-first century? **Climate Dynamics**, v. 29, n. April, p. 565–574, 2007.

RAIA, A.; ALBUQUERQUE CAVALCANTI, I. F. DE. The life cycle of the South American monsoon system. **Journal of Climate**, v. 21, n. 23, p. 6227–6246, 2008.

RAO, V. B.; HADA, K. Characteristics of rainfall over Brazil: Annual variations and connections with the Southern Oscillation. **Theoretical and Applied Climatology**, v. 42, p. 81–91, 1990.

RAYNER, N. A.; PARKER, D. E.; HORTON, E. B.; et al. Global analyses of sea surface temperature, sea ice, and night marine air temperature since the late Nineteenth Century. **jornal of geophysical research**, v. 108, 2003.

REBOITA, M. S.; AMBRIZZI, T.; ROCHA, R. P. DA. Relationship between the southern annular mode and southern hemisphere atmospheric systems. **Revista Brasileira de Meteorologia**, v. 24, p. 48–55, 2009.

REBOITA, M. S.; KRUSCHE, N.; AMBRIZZI, T.; ROCHA, R. P. DA. Entendendo o Tempo e o Clima na América do Sul. **Terrae Didática**, v. 8, n. 1, p. 34–50, 2012.

REYNOLDS, R. W.; SMITH, T. M. A High-Resolution Global Sea Surface Temperature Climatology. **Journal of Climate**, 1995. Disponível em:

<http://journals.ametsoc.org/doi/abs/10.1175/1520-0442(1995)008<1571:AHRGSS>2.0.CO;2\nhttp://journals.ametsoc.org/doi/abs/10.1175/1520-0442(1995)008<1571:AHRGSS>2.0.CO;2>. .

RICHTER, I.; XIE, S. P.; WITTENBERG, A. T.; MASUMOTO, Y. Tropical Atlantic biases and their relation to surface wind stress and terrestrial precipitation. **Climate Dynamics**, v. 38, n. 5-6, p. 985–1001, 2012.

RIENECKER, M.; SUAREZ, M.; TODLING, R.; et al. The GEOS-5 Data Assimilation System-Documentation of Versions 5.0. 1, 5.1. 0, and 5.2. 0. **Technical Report Series on Global Modeling and Data Assimilation**, v. 27, 2008.

RUIQING, L.; SHIHUA, L.; BO, H.; TANHONG, G. Connections Between the South Asian Summer Monsoon and the Tropical Sea Surface Temperature in CMIP5. **JOURNAL OF METEOROLOGICAL RESEARCH**, v. 29, n. 973, p. 106–118, 2015.

SAHA, S.; MOORTHI, S.; PAN, H. L.; et al. The NCEP climate forecast system reanalysis. **Bulletin of the American Meteorological Society**, v. 91, n. August, p. 1015–1057, 2010.

SAHA, S.; MOORTHI, S.; WU, X.; et al. The NCEP Climate Forecast System Version 2. **Journal of Climate**, v. 2, p. 1–61, 2013.

SANTOS, I. D. A.; FRANCO, N. J. D. N. Anomalias da precipitação no Sul do Brasil e as teleconexões. **XVII Congresso Brasileiro de Agrometeorologia**, 2011.

SCOCCIMARRO, E.; GUALDI, S.; BELLUCCI, A.; et al. Effects of tropical cyclones on ocean heat transport in a high-resolution coupled general circulation model. **Journal of Climate**, v. 24, n. 16, p. 4368–4384, 2011.

SEGELE, Z. T.; RICHMAN, M. B.; LESLIE, L. M.; LAMB, P. J. Seasonal-to-Interannual Variability of Ethiopia/Horn of Africa Monsoon. Part II: Statistical Multimodel Ensemble Rainfall Predictions. **Journal of Climate**, v. 28, p. 3511–3536, 2015.

SHARMILA, S.; JOSEPH, S.; SAHAI, A. K.; ABHILASH, S.; CHATTOPADHYAY, R. Future projection of Indian summer monsoon variability under climate change scenario: An assessment from CMIP5 climate models. **Global and Planetary Change**, v. 124, p. 62–78, 2015.

SHENG-PING, H. Potential Connection between the Australian Summer Monsoon Circulation and Summer Precipitation over Central China. **Atmosphere and Oceanic Science Letters**, v. 8, p. 120–126, 2015.

SIKKA, D. R.; GADGIL, S. On the Maximum Cloud Zone and the ITCZ over Indian, Longitudes during the Southwest Monsoon. **Monthly Weather Review**, 1980.

SILVA, A. R. Ciclo de vida do sistema de monção da América do Sul: Observação e simulação. **Tese de Doutorado**, 2008.

SONG, F.; ZHOU, T. Interannual variability of East Asian summer monsoon simulated by CMIP3 and CMIP5 AGCMs: Skill dependence on Indian Ocean-western pacific anticyclone teleconnection. **Journal of Climate**, v. 27, n. 4, p. 1679–1697, 2014.

SPERBER, K. R.; ANNAMALAI, H.; KANG, I. S.; et al. **The Asian summer monsoon: An intercomparison of CMIP5 vs. CMIP3 simulations of the late 20th century**. Climate Dynamics, 2013.

SRIVASTAVA, A K.; RAJEEVAN, M.; KSHIRSAGAR, S. R. Development of a high resolution daily gridded temperature data set (1969 – 2005) for the Indian region. **Atmospheric Science Letters**, v. 10, n. October, p. 249–254, 2009.

SULTAN, B.; JANICOT, S. The West African monsoon dynamics. Part II: The “preonset” and “onset” of the summer monsoon. **Journal of Climate**, v. 16, n. 21, p. 3407–3427, 2003.

TAPIADOR, F. J.; TURK, F. J.; PETERSEN, W.; et al. Global precipitation measurement: Methods, datasets and applications. **Atmospheric Research**, v. 104-105, p. 70–97, 2012. Elsevier B.V. Disponível em: <http://dx.doi.org/10.1016/j.atmosres.2011.10.021>. .

TAYLOR, K. E.; STOUFFER, R. J.; MEEHL, G. A. A Summary of the CMIP5 Experiment Design. , v. 4, p. 1–33, 2009. Disponível em: <http://cmip-pcmdi.llnl.gov/cmip5/docs/Taylor_CMIP5_design.pdf>. .

TAYLOR, K. E.; STOUFFER, R. J.; MEEHL, G. A. An overview of CMIP5 and the experiment design. **Bulletin of the American Meteorological Society**, v. 93, n. april, p. 485–498, 2012a.

TAYLOR, K. E.; STOUFFER, R. J.; MEEHL, G. A. An overview of CMIP5 and the experiment design. **Bulletin of the American Meteorological Society**, v. 93, p. 485–498, 2012b.

THOMPSON, D. W. J.; WALLACE, J. M. Annular Mode in the Extratropical Circulation. Part I : Month-to-Month Variability. **Journal of Climate**, v. 13, p. 1000–1016, 2000.

TRENBERTH, K. E.; STEPANIAK, D. P.; CARON, J. M. The global monsoon as seen through the divergent atmospheric circulation. **Journal of Climate**, v. 13, n. 22, p. 3969–3993, 2000.

VASCONCELLOS, F. C.; CAVALCANTI, I. F. A. Extreme precipitation over Southeastern Brazil in the austral summer and relations with the Southern Hemisphere annular mode. **Atmospheric Science Letters**, v. 11, p. 21–26, 2010.

VEIGA, J. A. P.; MARENGO, J. A.; RAO, V. B. A influencia das anomalias de TSM dos oceanos Pacífico e Atlântico sobre as chuvas de monção da AS. **Revista Brasileira de Meteorologia**, v. 17, p. 181–194, 2002.

WANG, B.; DING, Q. Global monsoon: Dominant mode of annual variation in the tropics. **Dynamics of Atmospheres and Oceans**, v. 44, n. 3-4, p. 165–183, 2008.

WANG, B.; LIU, J.; KIM, H. J.; WEBSTER, P. J.; YIM, S. Y. Recent change of the global monsoon precipitation (1979-2008). **Climate Dynamics**, v. 39, n. 5, p. 1123–1135, 2012.

WANG, B.; YIM, S. Y.; LEE, J. Y.; LIU, J.; HA, K. J. Future change of Asian-Australian monsoon under RCP 4.5 anthropogenic warming scenario. **Climate Dynamics**, v. 42, n. 1-2, p. 83–100, 2014.

WANG, P. Global monsoon in a geological perspective. **Chinese Science Bulletin**, v. 54, n. 7, 2009.

WATANABE, M.; SUZUKI, T.; O'ISHI, R.; et al. Improved climate simulation by MIROC5: Mean states, variability, and climate sensitivity. **Journal of Climate**, v. 23, p. 6312–6335, 2010.

WEBSTER, P. J.; MAGAÑA, V. O.; PALMER, T. N.; et al. Monsoons: Processes, predictability, and the prospects for prediction. **Journal of Geophysical Research**, v. 103, 1998.

WILKS, D. S. **Statistical Methods in the Atmospheric Sciences**. 2006.

WU, R. Possible roles of regional SST anomalies in long-term changes in the relationship between the Indian and Australian summer monsoon rainfall. **Theoretical and Applied Climatology**, 2015. Disponível em: <http://link.springer.com/10.1007/s00704-015-1443-9>. .

WU, R.; KIRTMAN, B. P. Roles of the Indian Ocean in the Australian summer monsoon-ENSO relationship. **Journal of Climate**, v. 20, n. 18, p. 4768–4788, 2007.

XIN, X.-G.; WU, T.-W.; ZHANG, J. Introduction of CMIP5 Experiments Carried out with the Climate System Models of Beijing Climate Center. **Advances in Climate Change Research**, v. 4, n. 1, p. 41–49, 2013.

XUE, F.; WANG, H.; HE, J. Interannual Variability of Mascarene High and Australian High and Their Influences on East Asian Summer Monsoon. **Journal of the Meteorological Society of Japan**, v. 82, n. 4, p. 1173–1186, 2004.

YIHUI, D.; YANJU, L. I. U.; YAFANG, S.; JIN, Z. From MONEX to the Global Monsoon : A Review of Monsoon System Research. **Advances in Atmospheric Sciences**, v. 32, p. 10–31, 2015.

YIM, S.-Y.; WANG, B.; LIU, J.; WU, Z. A comparison of regional monsoon variability using monsoon indices. **Climate Dynamics**, v. 43, p. 1423–1437, 2013.

YUE, S.; PILON, P.; CAVADIAS, G. Power of the Mann-Kendall and Spearman's rho tests for detecting monotonic trends in hydrological series. **Journal of Hydrology**, v. 259, n. 1-4, p. 254–271, 2002.

YUKIMOTO, S.; YOSHIMURA, H.; HOSAKA, M.; et al. Meteorological Research Institute-Earth System Model Version 1 (MRI-ESM1). **Technical Reports**, v. 64, n. 64, p. 88, 2011.

YULIHASTIN, E.; HERMAWAN, E. Annual Migration of Monsoon Over Indonesia Maritime Continent Based on OLR Data. , v. 35, n. 3, p. 27–39, 2012.

ZAMBONI, L.; KUCHARSKI, F.; MECHOSO, C. R. Seasonal variations of the links between the interannual variability of South America and the South Pacific. **Climate Dynamics**, v. 38, p. 2115–2129, 2012.

ZHANG, S.; WANG, B. Global summer monsoon rainy seasons. **International Journal of Climatology**, 2008. Disponível em: <http://www3.interscience.wiley.com/journal/4735/home>. .

ZHISHENG, A.; GUOXIONG, W.; JIANPING, L.; et al. Global Monsoon Dynamics and Climate Change. **Annual Review of Earth and Planetary Sciences**, v. 43, n. 1, 2014.

ZHOU, J.; LAU, K. M. Does a monsoon climate exist over South America? **Journal of Climate**, v. 11, n. 5, p. 1020–1040, 1998.

CAPÍTULO 4

ARTIGO PROPOSTO

Variability of the South Hemisphere summer monsoon indices and Antartic Oscillation in CMIP5 climate models

V. Schumacher

Agricultural Engineering Department, Federal University of Viçosa, Brazil.

F. Justino

Agricultural Engineering Department, Federal University of Viçosa, Brazil.

ABSTRACT

The present study aims to evaluate the representation of the summer monsoon indices in the Southern Hemisphere based on climate models of CMIP5, for present-day conditions. Explore the mains differences and commonality among regional monsoon domains, further, investigate the relationship of the Antarctic Oscillation with the summer monsoon rainfall. Here we evaluated the skill of ten CMIP5 models to represent interannual variability of the regional monsoon circulation indices in Southern Hemisphere (selected based on literature) during austral summer. Our results suggest that the austral summer monsoon precipitation domains are commonly characterized with low pressure anomalies associated with low-level cyclonic circulation and sea surface temperature gradient. The association between summer monsoon indices shows a dipole low (high) pressure over South America (SA) and Australia (AUS), this contributes to seesaw effect of precipitation, with positive (negative) anomaly between SA (AUS). The Australia index plays role in the rains in the Southern Africa domain, reporting positive (negative) anomaly rainfall over region southern Madagascar and west (northern Madagascar and northeastern). Southern America index displays a dipole pattern of precipitation anomalies over SA associated with increased (decrease) rainfall over northeast-southeast Brazil (southern-west central of South America), strongly linked with subtropical high (low) anomalies pressure. This results show climate models' skill in representing regional monsoon variability.

1. Introduction

The monsoon system represent the dominant mode of climate variability in the tropics and is responsible for the majority of annual rainfall over tropical land, playing an essential role on the hydrological cycle and agriculture (Webster et al. 1998; Zhisheng et al. 2014). The traditional concept of global monsoon dynamics is characterized by annual reversal of surface winds, contrasting summer rainfall (Trenberth et al. 2000; Wang and Ding 2008; Wang et al. 2012; Zhisheng et al. 2014). Furthermore, the global monsoon has been described as a manifestation of the seasonal migration of the Intertropical Convergence Zone (ITCZ) (Sikka and Gadgil 1980; Asnani 1993; Reynolds and Smith 1995; Wang 2009).

The main difference between Northern Hemisphere (HN) and Southern Hemisphere (SH) summer monsoons is the enhanced land-ocean thermal contrast, in which the NH surface warming is higher than in the SH. Thus, cross-equatorial pressure gradients that drives low-level cross-equatorial flows, contributes to strengthening the NH monsoon (Wang et al. 2012). The drives the monsoon global are linked by amplified temperature change gradient between land and ocean in the Northern Hemisphere (NH) and subtropical highs and the east-west mass contrast between Southeast Pacific and tropical Indian Ocean in the Southern Hemisphere (SH) (Liu et al. 2012).

The SH monsoon domains consist of three regional monsoons as South American (SAM), southern African (SAF) and Australian (AUS) (Zhang and Wang 2008; Hirokazu and Akio 2014). The change in wind direction in SAM occur over central region and southeastern Brazil (Zhou and Lau 1998). These changes contribute to the increase of moisture flux from Amazonia and South Atlantic Ocean over southeastern Brazil, favoring the intensification of convection. The onset of the SAM comprises three stages, in which the rainfall begins over northwestern progresses to the south and southeast. This leads to the South Atlantic convergence zone (SACZ) establishment and precipitation increase (Nieto-Ferreira and Rickenbach 2011).

In SAF, the rainfall is highly seasonal, and starts progressively southeastward from the west coast of equatorial South Africa across the continent reaching Mozambique, another propagation occurs over Madagascar

and tropical Indian Ocean from November to February (Zhang and Wang 2008). The enhanced rainfall anomaly is associated with low-level cyclonic anomaly centered at Madagascar (Yim et al. 2014). The peak of the rainy season is similar to the onset phase, from January to February (Zhang and Wang 2008).

The monsoon in northern Australia is characterized by of seasonal reversal winds in late December, when the trade easterlies diminish, and the subtropical ridge retreats poleward (Hendon and Liebmann 1990). The onset and termination mechanisms of the Australian summer monsoon are strongly associated with the surface temperature changes over continent, resulting in sea level pressure (SLP) changes.

The climate variability in SH is tightly modulated by extratropical teleconnection of the Antarctic Oscillation (AAO) between the middle and high southern latitudes (Gong and Wang 1999; Thompson and Wallace 2000). These mode of the climate variability are linked with air-sea fluxes of heat and momentum, and wind driven circulation through midlatitude westerlies and tropical easterlies (Justino and Peltier 2008). The AAO is also associated with the intensity of the polar jet and migration of the subtropical upper-level jet (Carvalho et al. 2005). Furthermore, the El Niño Southern Oscillation (ENSO) relationship with the phases of the AAO occur through the Subtropical Jet. In El Niño years, the Subtropical Jet would be stronger at lower latitudes, contributing to the change of the AAO signal. The positive (negative) phase resemble La Niña phase (El Niño) (Carvalho et al. 2005). In addition, summer extreme precipitation is associated with anomalous circulation forced by a Pacific South America (PSA) like a wave train intensified by AAO (Vasconcellos and Cavalcanti 2010).

There are many indices in the literature that define characteristics of regional monsoons, to facilitate monitoring and predictability, especially they have been used to defined the onset and demise dates of monsoons and the intraseasonal/interannual variability of rainy season over different monsoon systems, based on precipitation (Nieto-Ferreira and Rickenbach 2011; Kitoh et al. 2013), circulation (Gan et al. 2006; Zhang and Wang 2008; Kajikawa et al. 2009), OLR (Gan et al. 2004; Yulihastin and Hermawan 2012), moisture transport (Silva 2008) and others variables (Srivastava et al. 2009), including unified regional monsoon indices (Yim et al. 2014). However, the skills of the

climate models to predict wind components is better than to predict precipitation, thus monsoon indices based on wind changes are more efficient and better represent large-scale monsoonal features (Gan et al. 2006; Kajikawa et al. 2009).

Extensive studies have been conducted to examine the skill of climate models in simulating the variability of summer monsoon rainfall based in indices and future projections (Wang et al. 2014; Sharmila et al. 2015; Parth Sarthi et al. 2015;). However, most efforts focuses on regional monsoon domains for the Northern Hemisphere, over Asian and Indian monsoon; much less modeling studies involving monsoon indices for the Southern Hemisphere has been devoted. Some studies suggest changes by the end of the 21st century, such as increase significantly of the precipitation over East Asian summer monsoon (6.4 %/ºC), while in AUS summer monsoon will increase 2.6%/ºC (Wang et al. 2014). The land monsoon domain over Asia will expand with 10.6% in extent, and also the increase of the percentage of local summer rainfall including some parts of the Asia, Africa, Australia, South America monsoon (Lee and Wang 2014). Monsoon retreat dates will delay, onset dates will either advance or no change, prolonging the monsoon seasons (Kitoh et al. 2013). In addition, surface evaporation will increases at a higher rate, resulting in a larger increase rainfall based in thermodynamic and dynamic effects (Endo and Kitoh 2014). Furthermore, the increase of the global monsoon precipitation can be attributed to increase of moisture convergence due increase evaporation and water vapor (Kitoh et al. 2013; Yim et al. 2014).

Global Circulation Models (GCMs) have contributed to improve our knowledge about global and regional climates. However, the current GCMs show large biases in estimating monsoonal precipitation, especially in the Asian monsoon (Sperber et al. 2013) and dry region such as middle eastern and western Europe (Wang et al. 2014). The fifth phase of the Coupled Model Intercomparison Project (CMIP5) (Taylor et al. 2012) has partially alleviated these systematic errors. The predictability and skill in the CMIP5 models have been analyzed using multimodels ensemble or historical runs, and decadal predictions from different models have not been widely explored. Hence, a more detailed evaluation of the representation of the summer monsoon indices for South Hemisphere as represented by the CMIP5 models is required for the

improvement of the model performance. Therefore, accurate prediction of summer monsoon rainfall is crucial to reducing the impact of extreme events and socio-economic mitigation.

Thus, the goal of this paper is to evaluate how well monsoon indices summer in SH is reproduced by the CMIP5 models. In section 2 we describe the model, data and methods employed. The results are analyzed in section 3: inter-comparison between modeling results and reanalysis fields. We also evaluate the predicted seasonal cycle in terms of amplitude based in harmonic analysis. Analyze the interannual variability of summer monsoon indices, through correlation between summer monsoon indices with precipitation, sea level pressure and sea surface temperature. In addition, we assessed the response of the indices and the summer monsoon rainfall with the Antarctic Oscillation. Finally, in section 4, we discuss and summarize the principal findings of our analysis.

2. Data and Methodology

2.1 CMIP5 models and experiments.

The GCMs applied in this study are part of the Coupled Model Intercomparison Project Phase 5 - CMIP5 used in the Fifth Intergovernmental Panel on Climate Change (AR/5 IPCC) (Taylor et al. 2009, 2012). CMIP5 data are available at the Program Climate Model Diagnosis and Intercomparison (PCMDI) website (http://pcmdi9.llnl.gov/). We examined the 30-yr (1981-2010) decadal hindcasts conducted by ten GCMs and modeling centers, and selected models with the same time series, ensemble, type of experiment and only one model relating to each center modeling. For each model, only one ensemble member (r1i1p1) run has been used. The experiment consists of simulations over 10 year period that are initialized every five years (Taylor et al. 2012). The description and references for each of these models are given in Table 1.

2.2. Reanalysis Datasets and modeling evaluation

To evaluate the reliability of the CMIP5 simulations, they have been compared with the Climate Forecast System Reanalysis (CFSR) (Saha et al. 2010). CFSR data has a spatial resolution of 0.5º latitude and longitude from "http://cfs.ncep.noaa.gov/cfsr/". Reanalysis products are usually used to perform hindcast analysis by the inclusion of observations, data assimilation techniques and numerical methods (Tapiador et al. 2012). For reference of precipitation data were used reconstructed monthly precipitation dataset, encompassing observed data from pluviometers and remote sensing, provided by the Global Precipitation Climatology Project (GPCP) (Adler et al. 2003), with 2.5ºx 2.5º gridded from "http://www.esrl.noaa.gov/psd/". And for sea surface temperature (SST) by Hadley Centre Sea Ice and Sea Surface Temperature (HadISST) (Rayner et al. 2003), from "http://www.metoffice.gov.uk/hadobs/hadisst/".

For both, CMIP5 models and observed datasets we examined monthly mean of precipitation (PR), surface temperature (ST), sea surface temperature (SST), sea level of the pressure (SLP), components of the zonal wind (Us) and meridional wind (Vs) for present-day (PD) simulations (1981-2010) over SH. The models and reanalysis datasets were regridded to common 2º latitude by 2º longitude grid through bilinear interpolation for comparison.

Table 1: General description of the CMIP5 models used in this study.

Models	Modeling Center	Country	AGCM resolution	References
BCC-CSM1.1	BCC	China	2.8º x 2.8º	(Xin et al. 2013)
CanCM4	CCCma	Canada	2.8º x 2.8º	(Chylek et al. 2011)
CFSv2-2011	COLA/NCEP	USA	1º x 1º	(Saha et al. 2013)
CMCC	CMCC	Italy	2º x 2º	(Scoccimarro et al. 2011)
GEOS-5	NASA GMAO	USA	2º x 2.5º	(Rienecker et al. 2008)
GFDL-CM2.1	NOAA GFDL	USA	2º x 2.5º	(Delworth et al. 2006)
IPSL-CM5A-LR	IPSL	France	1.9º x 3.7º	(Dufresne et al. 2013)
MIROC5	MIROC	Japan	1.5º x 1.5º	(Watanabe et al. 2010)
MPI-ESM-LR	MPI-M	Germany	1.8º x 1.8º	(Raddatz et al. 2007)
MRI-CGCM3	MRI	Japan	1.8º x 2.8º	(Yukimoto et al. 2011)

Evaluations of these meteorological variables are crucial because they are tightly connected to the monsoonal system. To verify the GCMs capability in

simulating the PD climate, statistical significance of the differences were calculated by the t test. For precipitation nonparametric test Wilcoxon-Mann-Whitney (Wilks 2006) with a 95% confidence level is used. Seasonal spatial variability is analyzed based on harmonic analysis (Fourier transformation). The harmonic analysis can characterize different climate regimes and transitions regions (Jakubauskas et al. 2001). Moreover, it is possible to identifying dominant climate features in the spatial-temporal scales. Thus, climate features related to seasonality may be investigated in GCMs and reanalysis data.

The regional monsoon domains for SH (Figure 1) consists of South American monsoon – SAM, South African monsoon – SAF and Australian monsoon – AUS. These regions are characterized by a sharp contrast between the rainy summer and dry winter. The summer monsoon indices (SMIs) are calculated with respect to three dominant modes of monsoon, computed for all selected models for present day conditions, during austral summer (DJF), because these months represent the peak of the wet season related to monsoon domains in HS. The choice of SMIs used in this study is based on regional monsoon studies, which have been tested and proposed for studies of interannual variability of the monsoon activities.

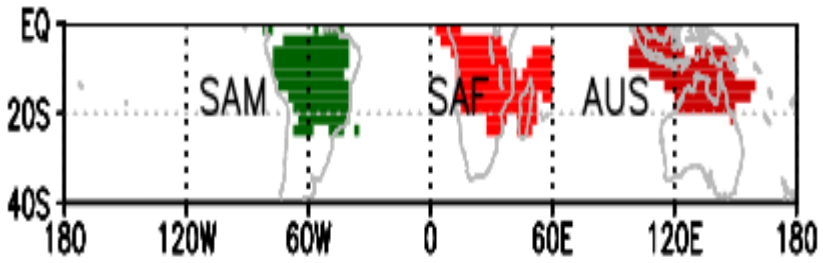

Figure 1 – Regional monsoon precipitation domains for South Hemisphere. Defined as where annual range (difference between November-March and May-September) of precipitation is greater than 2.5 mm/day, based on an observational GPCP data. Adopted from (Endo and Kitoh 2014).

The SMIs are defined as zonal and meridional index (UVI) for SAM domain. It is the sum of the 850-hPa zonal wind averaged in 10ºS-15ºS,60ºW-50ºW area and the 850-hPa meridional wind averaged in the 20ºS-25ºS,65ºW-60ºW. The UVI was proposed by Gan et al. (2006) to examine the influence of the moisture transport by the low-level jet on the eastern side of the Andes.

The Southern African index (SAFI) is defined as the difference of the zonal wind at 850 hPa between 5ºS-15ºS,20ºE-50ºE and 20ºS-30ºS,30ºE-55ºE areas, proposed by Yim et al. (2014). The SAFI is associated with low-level cyclonic anomaly centered at Madagascar, including part of Southwestern Indian Ocean and Tanzania-Mozambique.

The Australian monsoon index (AUSMI) is computed as 850 hPa zonal wind averaged over (5ºS-15ºS, 110ºE-130ºE) (Kajikawa et al. 2009). The AUSMI reflect intraseasonal, interannual and interdecadal variability time scales of the Australia monsoonal rainfall.

It is well known that in addition to the monsoonal climate, the SH exhibits other modes of climate variability. The leading teleconnection pattern in the subtropical atmospheric circulation in the Southern Hemisphere, defined by the AAO, is computed based on empirical orthogonal function (EOF) based on the covariance matrix, was apllied to the montly mean 500-hPa height anomalies poleward of 20º latitude for SH. The seasonal cycle was removed, and grid points were weighted by the square root of the cosine of latitude. The AAO is defined by the first mode from EOF.

To analyze the influence of AAO in monsoon rainfall in the SH was applied the composite or weighted average method, as described below:

$$\bar{x}_p = \frac{\sum_{j=1}^{k} xifi}{\sum_{j=1}^{k} fi}$$

$\bar{x}_p$ is the weighted average, xi is the values of the precipitation (DJF), and fi the indice values (AAO-DJF). The numerator responds to the sum of the product between the precipitation and the AAO indice, and denominator by sum the values of the indice, separate in positive and negative about the variable, defined as the difference between the two weightings (positive-negative), allowing the identification of the variability of teleconnection on the variable in question regionally (SANTOS and FRANCO 2011; Campos 2013).

3. Results

3.1. Simulations of the variability climate in Southern Hemisphere by CMIP5

This section discusses intercomparison between CMIP5 results and the reanalysis fields in response to important variables simulations in variability of the monsoon domains and the SH climate. Annually zonally averaged were calculated to describe the behavior of the variables in relation to latitude over time. Here, we focus on comparing the differences between the models on the tropic, including Antarctic continent (0º-90ºS).

Figure 2a shows the annual zonally averaged surface temperature in SH. All models agree with CFSR results, with exception over the Antarctic continent, below 60°S latitude, in which the models differ to the reanalysis. The CFSv2-2011 and MIROC5-MRI-GCCM3 models simulate the largest bias temperature over Antarctic, around 22 K and 10 K respectively. The majority of the models have higher temperature, solely CMCC-CM, GEOS-5, MPI-ESM-LR have values lower than CFSR. Some evidences have been founded that problem of representing the step topography by GCMs may be the cause of these discrepancies (Justino et al. 2011). The model that best represent the pattern temperature is CanCM4.

CMIP5 models reproduce similar pattern of precipitation by GPCP dataset (Figure 2b). However, all models overestimate precipitation in the tropic. The IPSL-CM5A-LR shows the largest values, in the tropic and subtropical region. MRI-CGCM3 shows a peak rainfall over 10ºS of up 3 mm/day as compared to GPCP dataset. The CMCC-CM reproduce the average annual cycle of precipitation in the subtropics, and CanCM4 is the model that is closest of the observed pattern.

The zonal pattern of surface winds reproduced by CMIP5 are shown in Figure 2c. Most models exhibit an advance over the latitude (0º-70ºS) for zonal wind compared to CFSR, main the IPSL-CM5A-LR and BCC-CSM1.1 models. All models reproduce well the zonal wind over Antarctic continent, although all models are weaker than CFSR dataset between 80ºS-40ºS, and more intense in the region of the tropics (HS). MPI-ESM-LR is the best model that follows the pattern of the observed data over all latitudes. On the other hand, the models

do not reproduce well the surface meridional wind compared with reanalysis, only in the Antarctica region until 50ºS, overestimating the wind in this region.

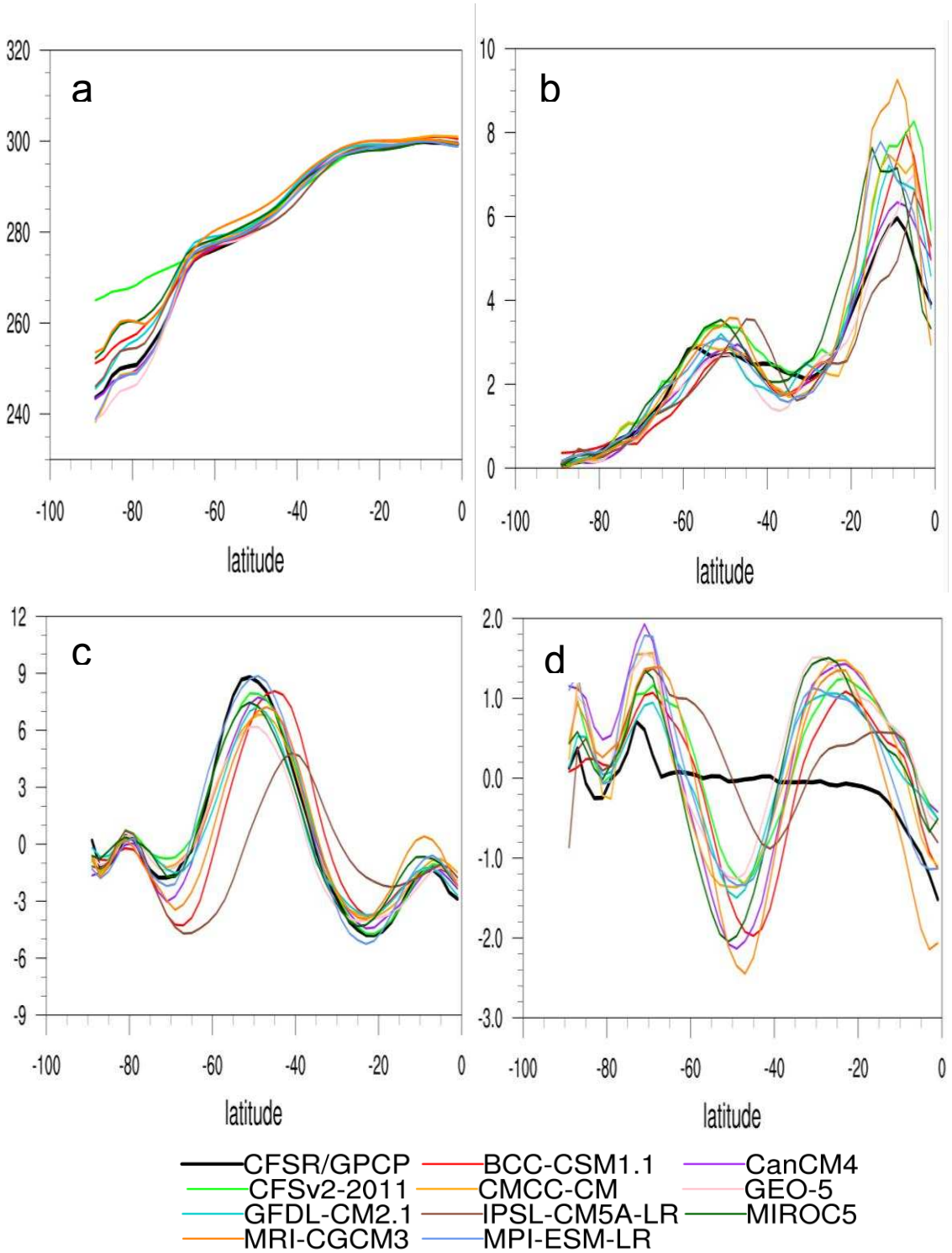

Figure 2- Annual zonally average of surface temperature (K) (a), precipitation (mm/day) (b), surface wind zonal (m/s) (c) in and surface meridional wind (m/s) in South Hemisphere (0º-90ºS,180ºW-180ºE) 1981-2010, for CFSR (black line) and CMIP5 models, except for precipitation GPCP (black line) used.

3.2. *Differences by CMIP5 in climate of the Southern Hemisphere*.

Figures 3-5 shows differences between CMIP5 models and reference datasets for the interval (1981-2010). The CMIP5 models exhibits a warm and cold bias over Antarctic of up 20 K and 12 K respective (Figure 3), for CFSv2-2011 and GEOS-5. Negative anomalies are also simulated over Antarctic by BCC-CSM1.1, CanCM4, CMCC-CM, GFDL-CM2.1, IPSL-CM5A-LR, MPI-ESM-LR and MRI-CGCM3, mainly over Wilkes land with 95% confidence interval. Only CanCM4, CMCC-CM, GFDL-CM2.1 and MRI-CGCM3 showed negative anomalies also over sea Weddell. The strong temperature gradient observed in CFSv2-2011 model on Antarctic and adjacent ocean compared to CFSR, is also seen in Figure 2a. For Australia continent solely GEOS-5 presented significant difference above 4 K while in Africa two models (CFSv2-2011 and GEOS-5) show positive anomalies on the whole continent. Over South America (SA) the CFSv2-2011 overestimate the temperature over the Andes by up 20 K and the models BCC-CSM1.1 and CanCM4 shows cold bias in southern South America. All models overestimate the temperature of the tropical Pacific, up to 4 K, only CFSv2-2011 shows negative values.

Monthly mean precipitation for SH by GPCP and difference of the precipitation between CMIP5 models and GPCP dataset is shows in Figure 5. Results indicate that all models are able to place the ITCZ, but they disagree on locating the maximum rainfall, only MIROC5 reproduced the position similar to the GPCP dataset. It should be noted that all models overestimate the precipitation in the equatorial zone in compared to other (Hirota and Takayabu 2013). CMIP5 models disagree more in reproduced precipitation over South America than Africa and Australia. CanCM4 displays larger differences the precipitation over the central part of the Amazon and north of SA, with anomaly negative of up 5 mm/day than GPCP reference, while GEOS-5 overestimate of the precipitation over east Argentina, Chile, north South America and Brazil. Positive anomalies across the African continent over the Congo rainforest and eastern region are observed in MIROC5, with 95% significance. In general, the models show the mean zonal field wind weaker that the observed CFSR dataset, for both the trade winds and to westerly winds (Figure 5). For meridional wind (not showed) display pattern positive anomalies over the Pacific, Atlantic and Indian oceans

at west of the continents of SA, Africa and Australia, and also in continent Antarctic, mainly near the Ross and Weddel seas.

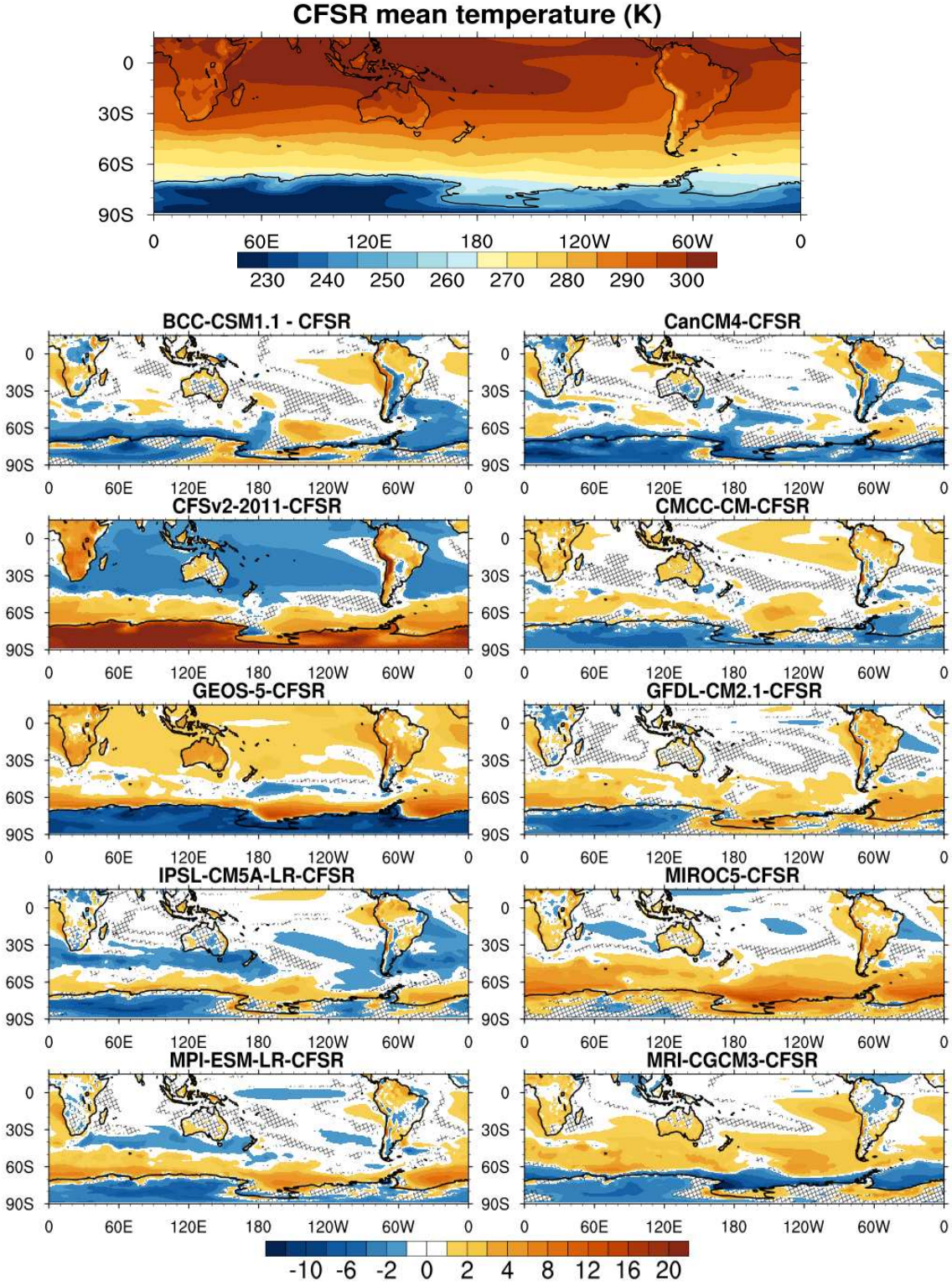

Figure 3- Monthly mean surface temperature (K) by CFSR. Difference of the monthly mean surface temperature between CMIP5 models and CFSR in 1981-2010. Regions without black grids are significant at 95% confidence level by test T.

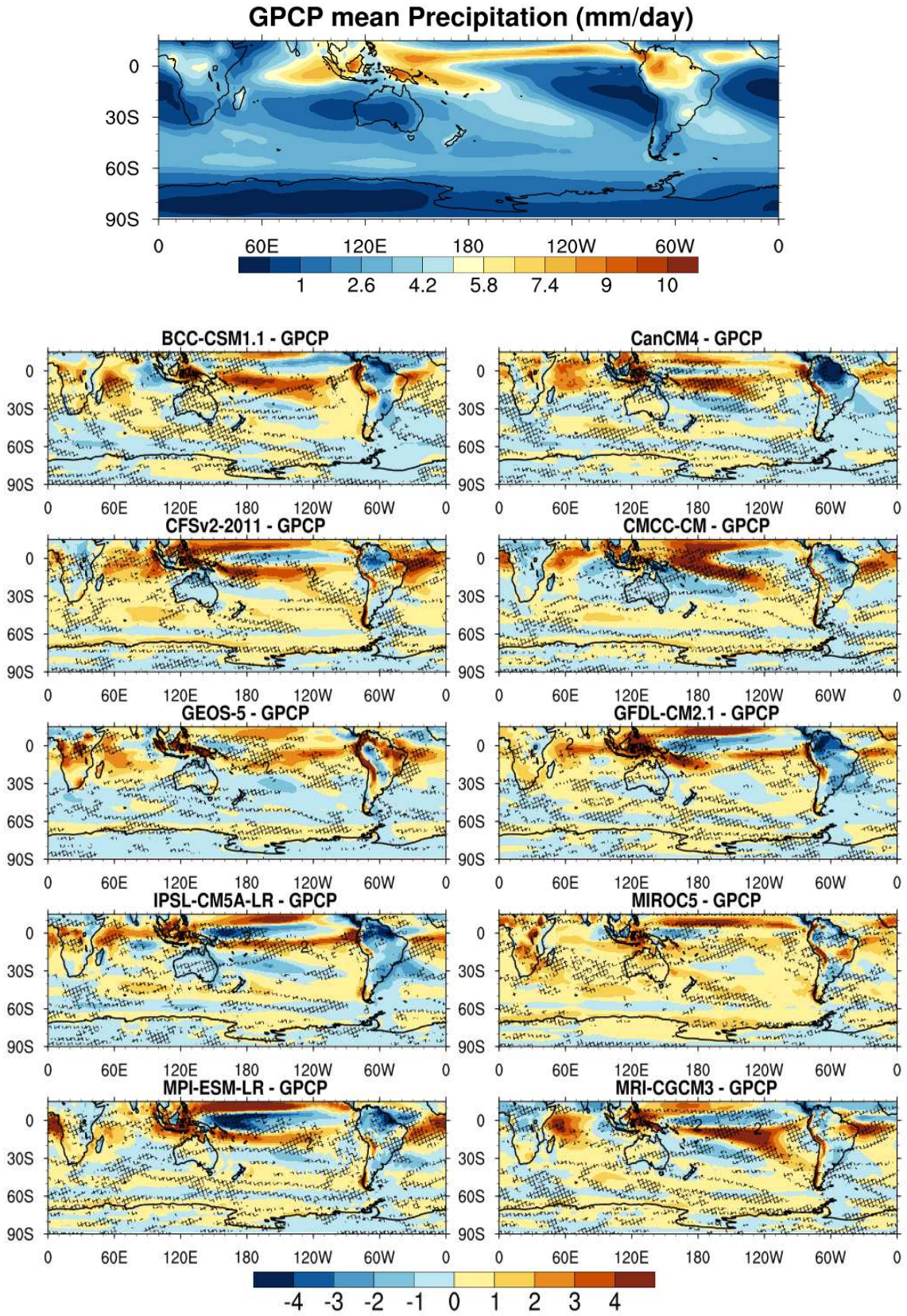

Figure 4- Monthly mean precipitation (mm/day) by GPCP. Difference of the precipitation between CMIP5 models and GPCP dataset. Regions without black grids are significant at 95% confidence level by test Wilcoxon-Mann-Whitney.

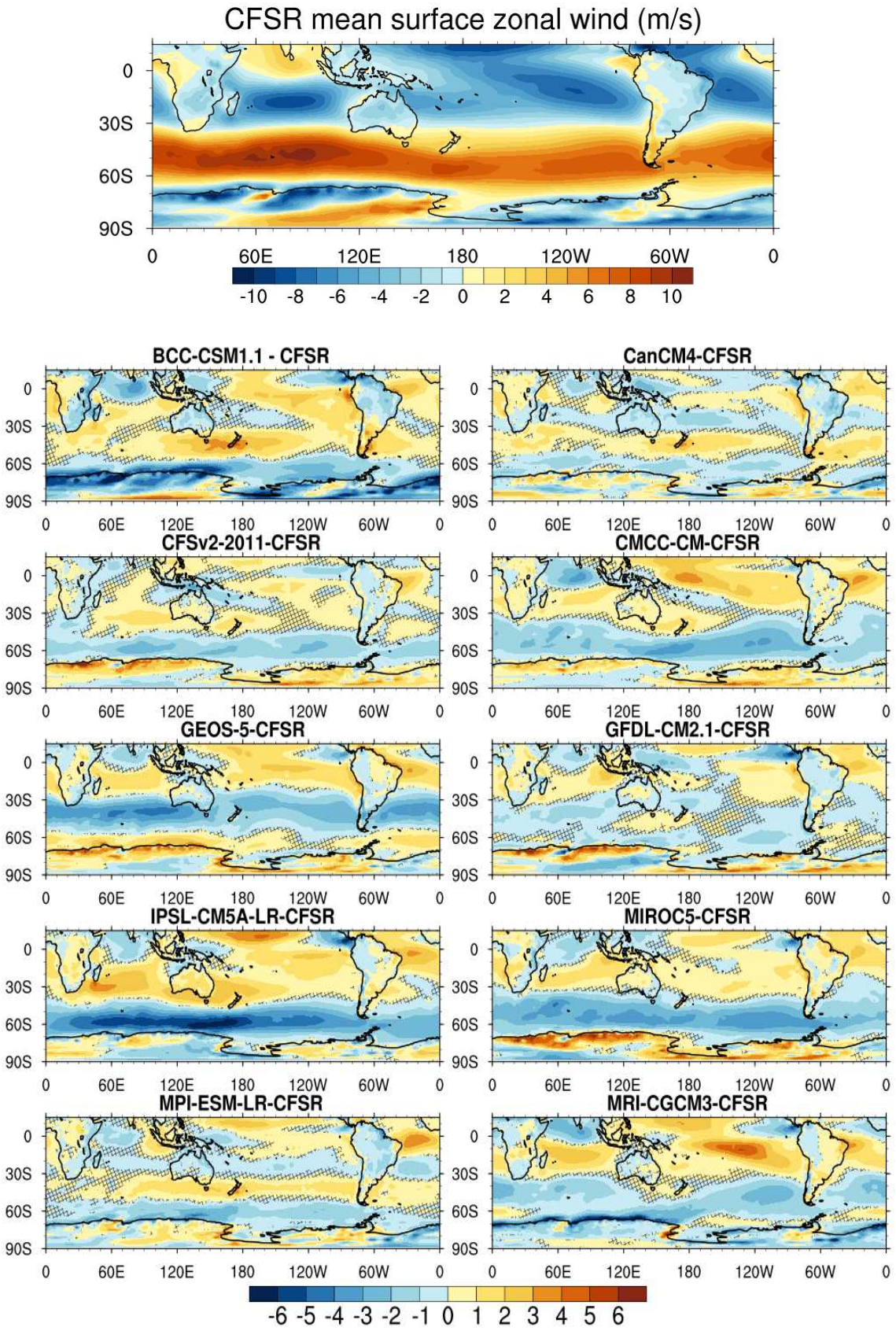

Figure 5- The same as Figure 3 except for monthly mean surface wind zonal (m/s) by CFSR. Difference of the surface wind zonal between CMIP5 models and CFSR dataset.

3.3. Seasonal Climate Cycle in Southern Hemisphere.

The magnitude of the seasonal cycle is evaluated in terms of the amplitude of harmonic analyzing, for the period 1981-2010. To identify if the ten selected models are able to realistically simulate the areas with the largest seasonal variability, differences of the first harmonic between all models and observation datasets are displayed in Figure 6, and the amplitude of the first harmonic of surface temperature based on CFSR. It is characterized by larger amplitude over Weddell and Ross seas in Antarctic. This can be associated with seasonal changes of sea ice due to radiative budget. Changes in the atmospheric inversion layer may play a role. The regions of the SAM, SAF and AUS also have higher variability. Comparison between the CMIP5 simulations and reanalysis data demonstrated that only MPI-ESM-LR and CMCC-CM satisfactorily simulated the spatial pattern of the first harmonic (not showed). The main differences between models and reference dataset are observed over the Antarctic continent and adjacent ocean for seven models (BCC-CSM1.1, CanCM4, GEOS-5, GFDL-CM2.1, IPSL-CM5A, MIROC5, MRI-CGCM3). The GFDL-CM2.1 also shows more variability over north of the SA, Australia and South Africa.

Amplitude of precipitation shows stronger seasonal cycle associated with ITCZ, and over north-central SA, Southern African and northern Australia (Figure 7), monsoon regions. The models GFDL-CM2.1, IPSL-CM5A-LR, MIROC5, MPI-ESM-LR and MRI-CGCM3 also reproduce maximum amplitude over monsoon domains showing the same pattern of CFSR. However, over African continent and SA the GCMs disagree, with large zonal variations of precipitation, overestimation over eastern tropical Atlantic and Pacific. In the Pacific this is associated with a misrepresentation of the cold tongue simulated by the CMIP3 models, discuss by Richter et al. (2012). In the Atlantic, the bias can be linked to the representation of the tropical Atlantic variability.

For the surface zonal wind regions higher amplitude is found over the Indian Ocean and Indonesia, the ITCZ is also observed short variability in Figure 8. All models are able to represent the same spatial pattern of the first amplitude observed in reanalysis datasets (not showed). The differences between CMIP5 and CFSR (Figure 8) show positive amplitude up 4 m/s over Antartic for BCC-

CSM1.1 and MRI-CGCM3. Main differences are observed on ocean Indian eastern coast of Africa and Indonesia. For surface meridional wind shows more variability over Congo rainforest and over ocean Indian eastern coast of Africa (not showed).

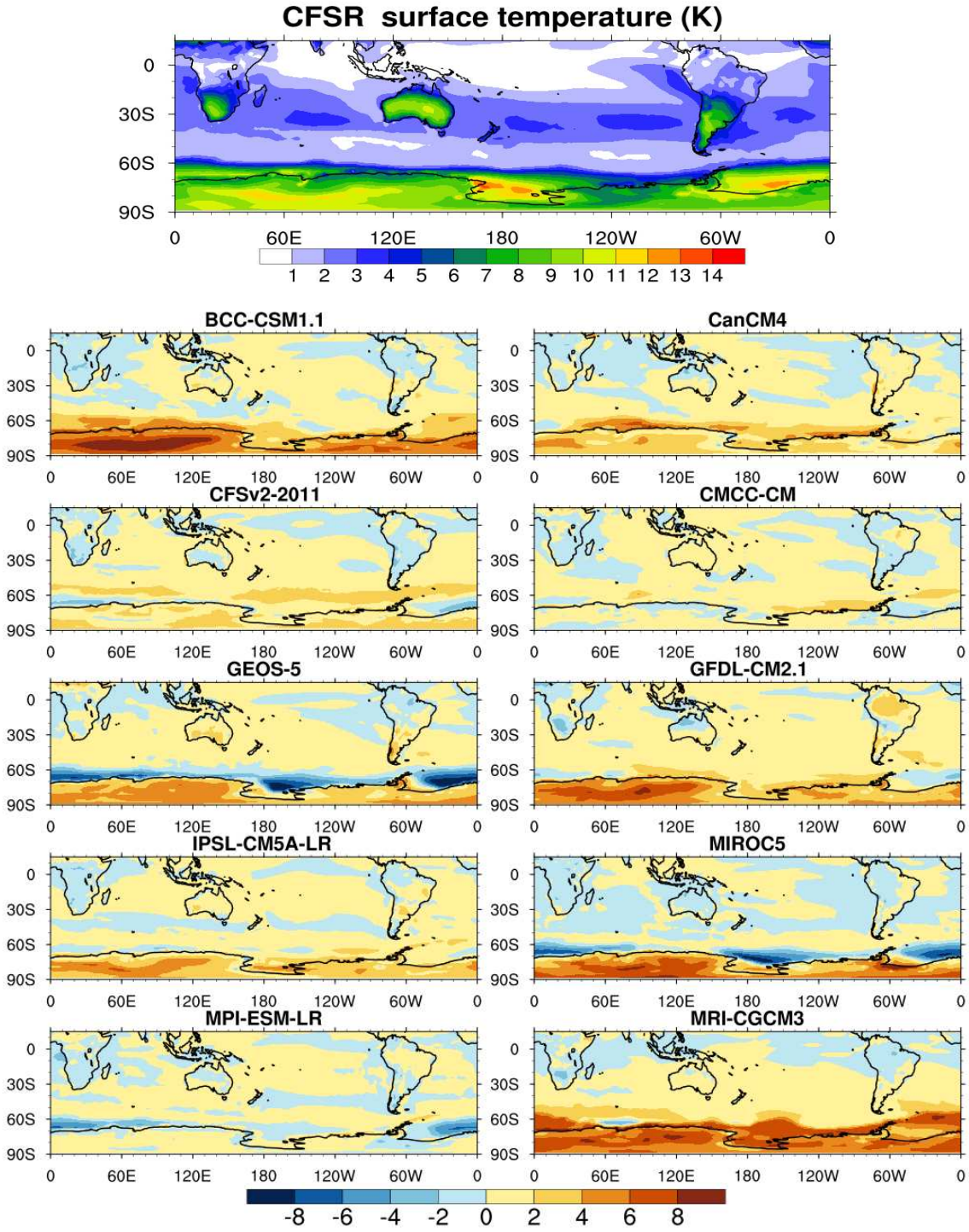

Figure 6- Amplitude of the first harmonic of surface temperature (K) from CFSR. Anomalies between CFSR and CMIP5 models for amplitude of the first harmonic of surface temperature.

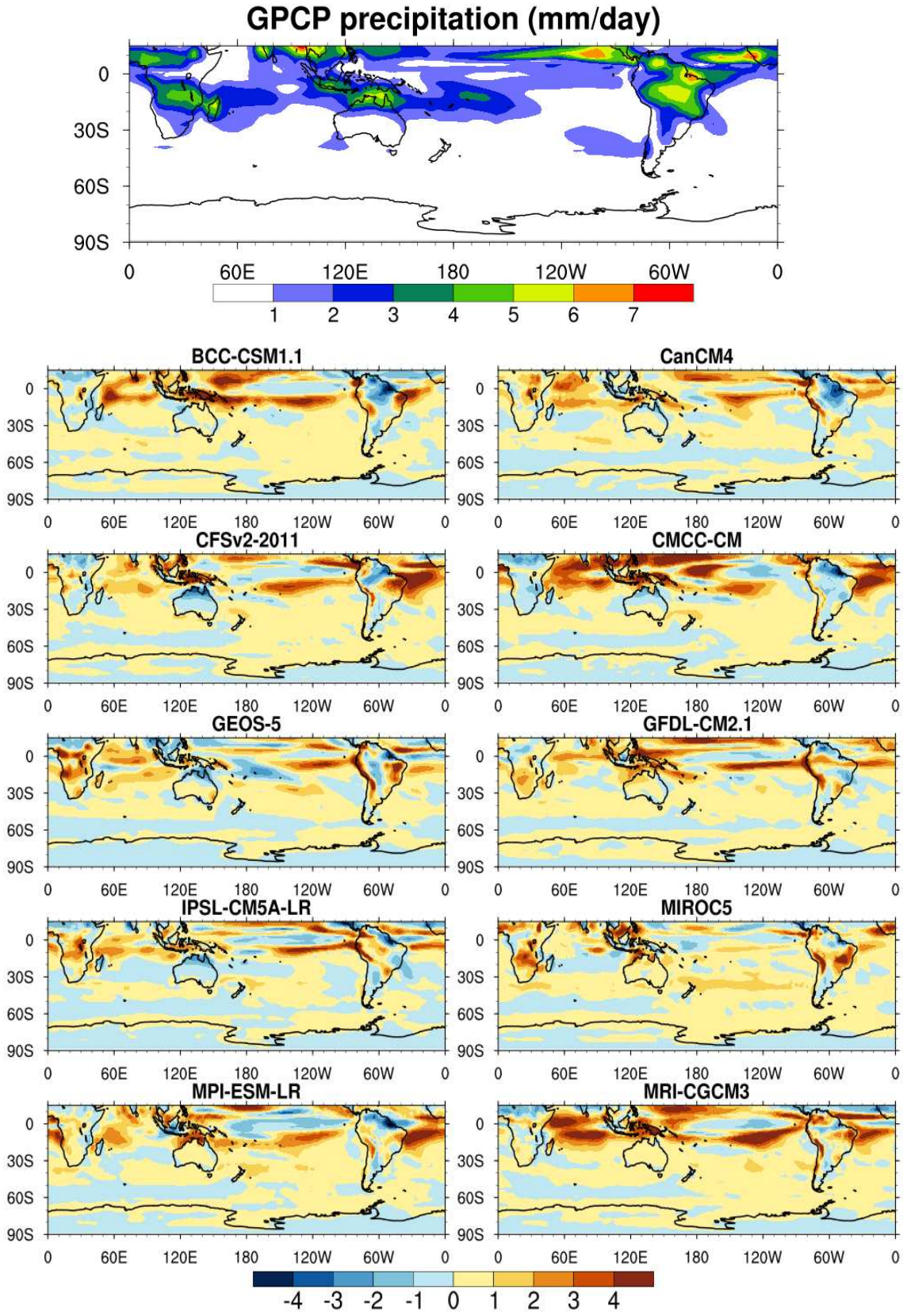

Figure 7- Amplitude of the first harmonic of precipitation (mm/day) by GPCP. Anomaly between GPCP and CMIP5 models for amplitude of the first harmonic of precipitation.

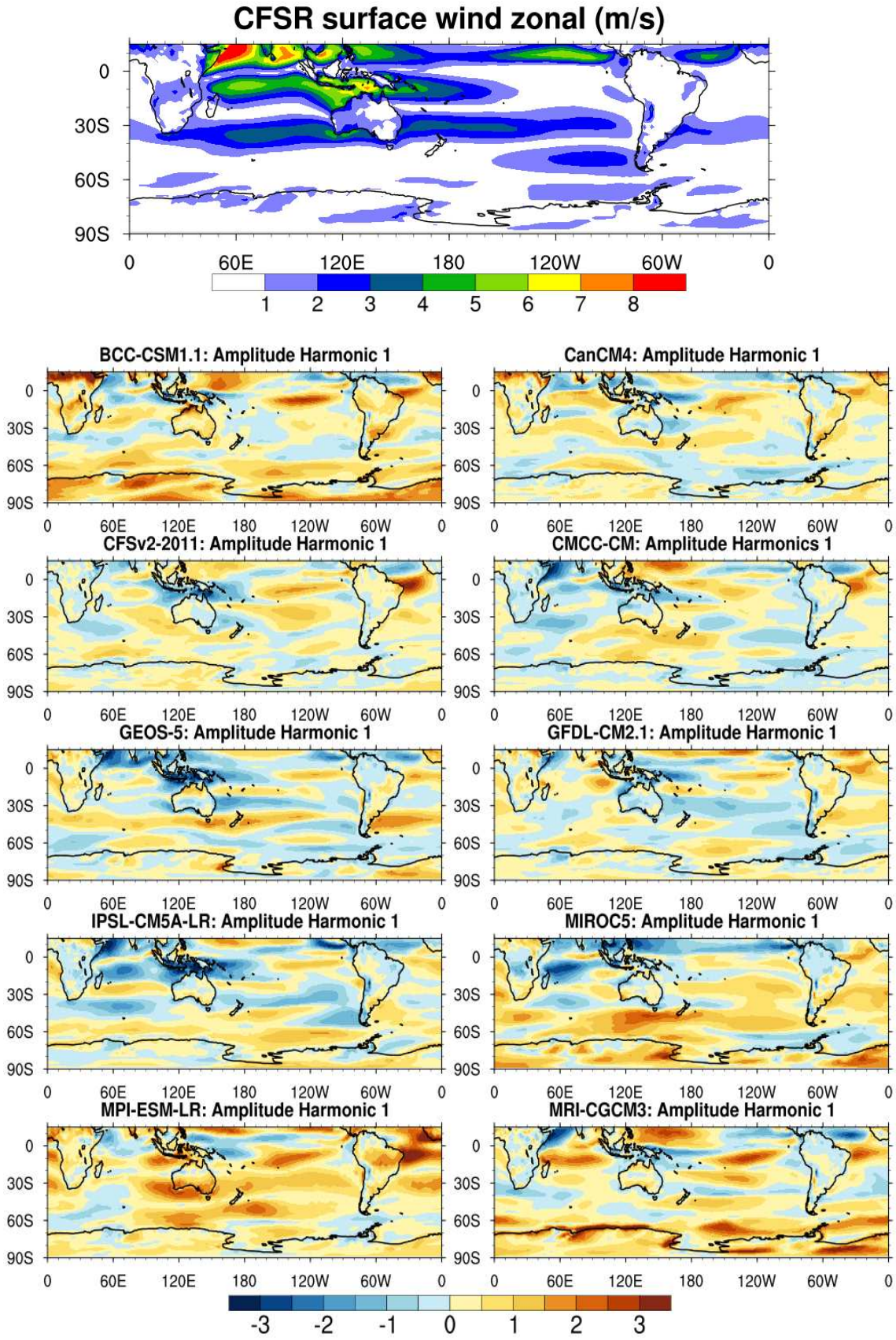

Figure 8- Amplitude of the first harmonic of surface zonal wind (m/s) by CFSR. Anomaly between CFSR and CMIP5 models for amplitude of the first harmonic of surface zonal wind.

3.4. Seasonal Cycle in Monsoon Domain of the Southern Hemisphere

The seasonality of the regional monsoon in SH are depicted by the Hovmöller Diagram to explore the main differences and variability simulated by climate models encompassing tropical region (0º-30ºS,180ºW-180ºE).

The zonal mean surface temperature (Figure 9a) exhibits a greater seasonal variability over monsoon domains SAM (60ºW-50ºW), SAF (25ºE-60ºE) and AUS (110ºE-150ºE), with higher gradients between summer and winter over AUS by CFSR dataset. The CFSv2-2011 model displays a cold bias over all longitude area, mainly in June-October, and warmer in the spring and summer seasons in relation to CFSR.

Hovmöller diagrams for precipitation (Figure 9b) is observed the wet season cycle well defined for the SAM domain, starting in November and ending March -April, with peaking in the months from December to February. On the other hand, for the SAF it is not very clear, although it can be seen that the peak of the rainfall also occurs between December to February, the same is observed for the AUS by GPCP dataset. The BCC-CSM1.1, CanCM4, GFDL-CM2.1 and MPI-ESM-LR models, overestimate the precipitation over AUS.

For component of zonal wind at 850 hPa observed change in the direction of westerly winds to eastward from the end of November-December, clearer to longitude comprising AUS. For other domains also are noted easterly winds especially during austral summer. Most models overestimate the easterly winds, especially over regions of SAF and AUS, with exception of the CMCC-CM and CFSv2-2011 which have weaker winds (Figure 9c).

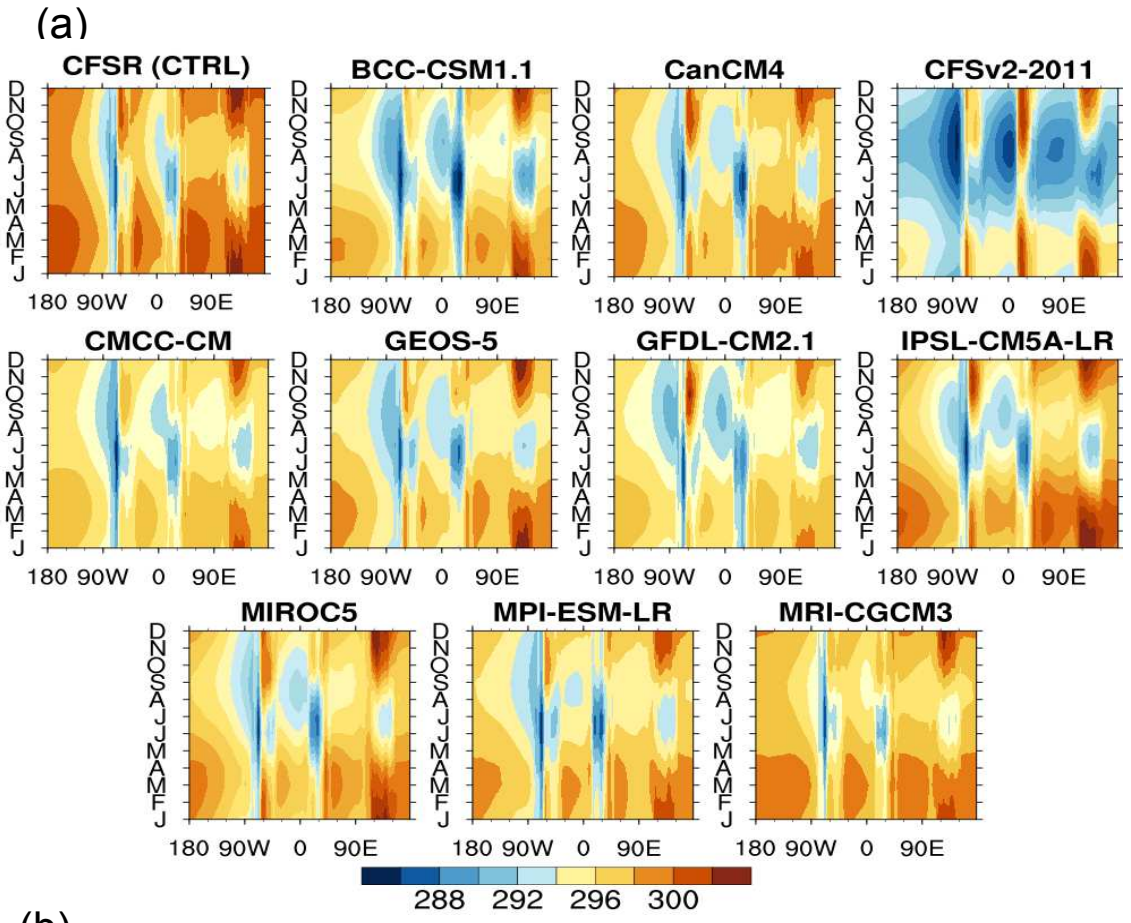
(a)
CFSR (CTRL)
BCC-CSM1.1
CanCM4
CFSv2-2011
CMCC-CM
GEOS-5
GFDL-CM2.1
IPSL-CM5A-LR
MIROC5
MPI-ESM-LR
MRI-CGCM3
D N O S A J J M A M F J
180 90W 0 90E
288 292 296 300

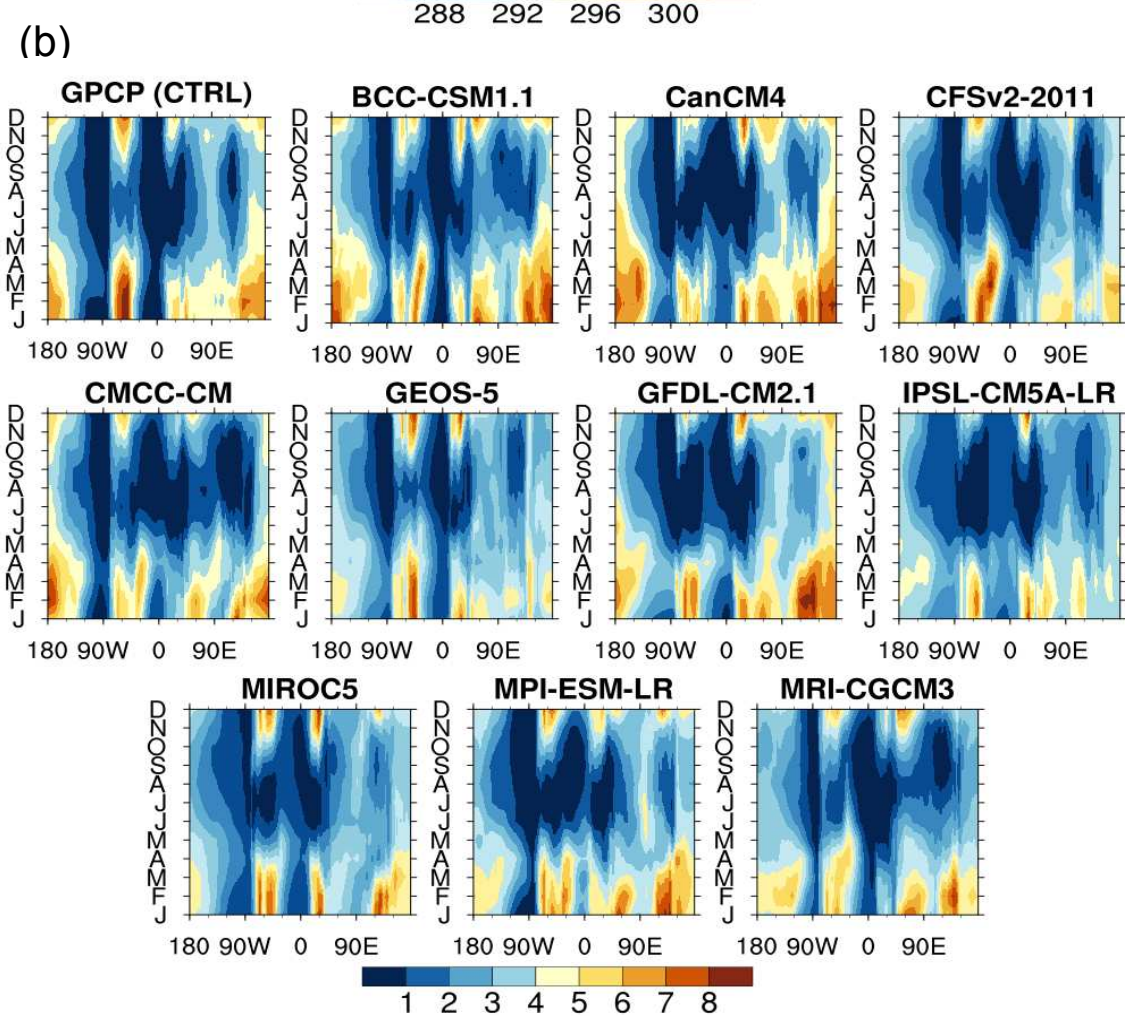
(b)
GPCP (CTRL)
BCC-CSM1.1
CanCM4
CFSv2-2011
CMCC-CM
GEOS-5
GFDL-CM2.1
IPSL-CM5A-LR
MIROC5
MPI-ESM-LR
MRI-CGCM3
D N O S A J J M A M F J
180 90W 0 90E
1 2 3 4 5 6 7 8

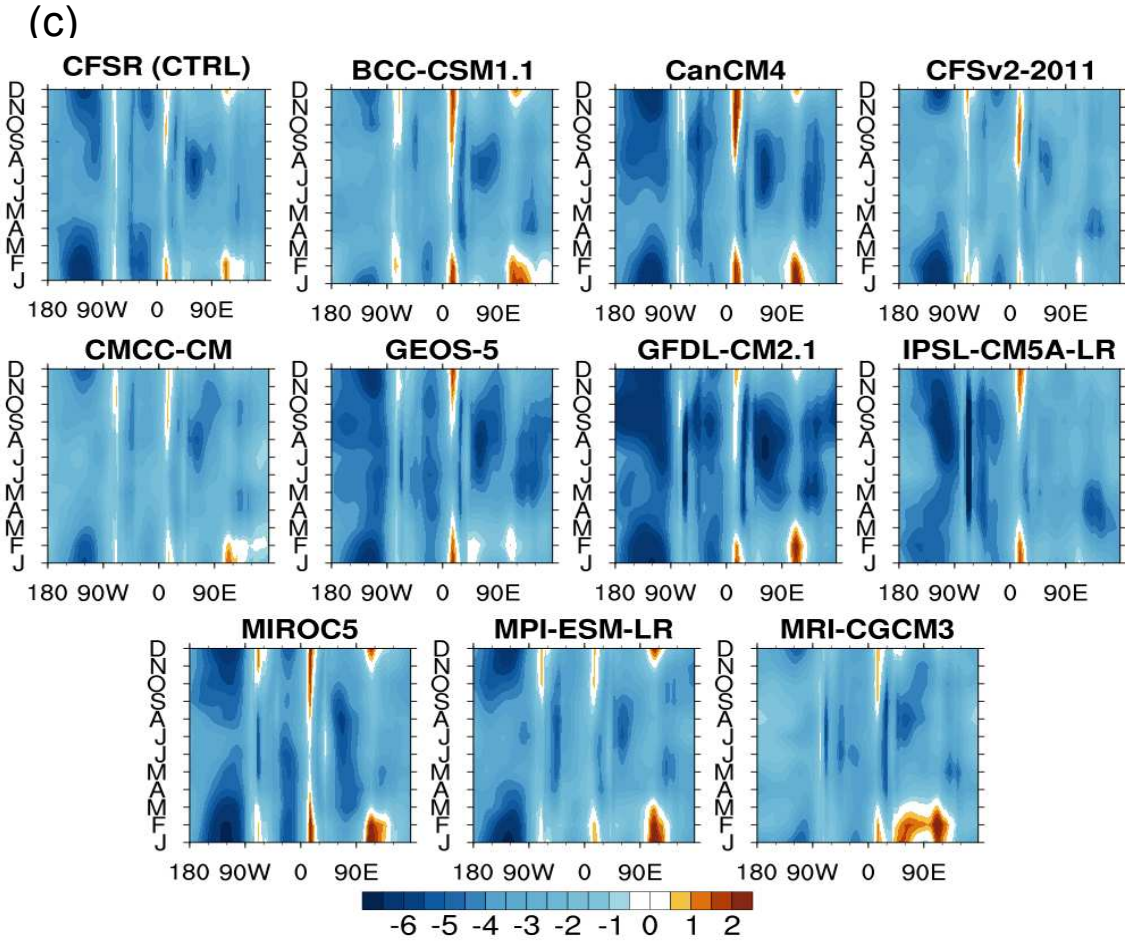

Figure 9 - Longitude-time Hovmöller Diagrams for zonal mean surface temperature (K) (a), precipitation (mm/day) (b) and zonal wind at 850 hPa (m/s) (c) in tropical region in SH (0º-30ºS,-180ºW-180ºE), 1981-2010. The CFSR and GPCP are used as control (CTRL).

3.4 Summer monsoon indices

To evaluate the applicability of the SMIs based on the wind with the rainfall in the respective domains monsoon, summer monsoon rainfall indices (SMRIs) was computed to comparison. The SMRIs are defined as the area averaged precipitation rate (mm/day) during austral summer (DJF), corresponding to each rectangular regional domains (Figure 10). The rectangular domain represents the regional monsoon precipitation domains present in Figure 1, according to Yim et al. (2014). However, for the SAM domain includes a portion strongly related with mean annual cycle of circulation, proposed by Gan et al. (2006). Statistical significance of the SMIs and SMRIs trend by Mann-Kendall rank statistics (Yue et al. 2002; Wilks 2006), showed no trend in the analyzed period (1981-2010).

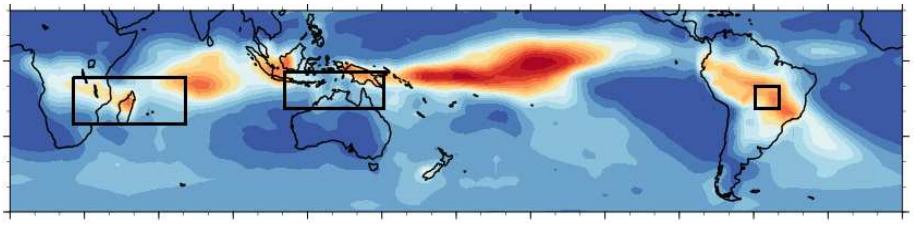

Figure 10- Regional summer monsoon rainfall indices (mm/day) in the rectangular domains to represent the respective tropical monsoon domains in SH. The dimensions latitude and longitude corresponding to each rectangular box are displayed in Table 2.

Table 2 shows the correlation coefficients (CCs) between the SMRIs and SMIs over each regional domain. The precipitation and circulation indices are significantly correlated, with CC of 0.51 for SAM, to SAF domain the CC found in this study (0.64) is smaller than proposed by Yim et al. (2014), however, we consider here DJF as austral summer, unlike calculated by the authors (0.71 - DJFM), and for AUS domain 0.85, the same found by Kajikawa et al. (2009), although the domain of the SMIRs is not the same. This suggests that the SMIs based in wind responds well the regional monsoon rainfall variability.

To analyze the relationship of the indices based on wind with rainfall in regional domain monsoon, the time-series between SMRIs and SMIs is shown in Figure 11. It is noticed that the more positive (negative) the SMIs higher (smallest) is precipitation anomalies, i.e., rain above (below) the average. It is interesting to note that the AUSMI shows a peak with negative values in 1983, associated with strong El Niño event, as seen in section 3.7. Moreover, it is noted that strong precipitation anomalies are linked with La Niña events, e. g. peaks observed in 2007-2008, more evident on the SAF.

Table 2 - The correlation coefficients between the regional summer monsoon rainfall - SMRIs and summer monsoon indices - SMIs.

Regional Monsoon	Monsoon domain SMIRs	Monsoon domain SMIs	CC
SAM	(10ºS-20ºS,60ºW-50ºW)	(10ºS-15ºS,60ºW-50ºW) (20ºS-25ºS,65ºW-60ºW)	0.51
SAF	(7.5ºS-25ºS,25ºE-70ºE)	(5ºS-15ºS,20ºE-50ºE) (20ºS-30ºS,30ºE-55ºE)	0.64
AUS	(5ºS-20ºS,110ºE-150ºE)	(5ºS-15ºS,110ºE-130ºE)	0.85

The CCs represent significant at 99% confidence level.

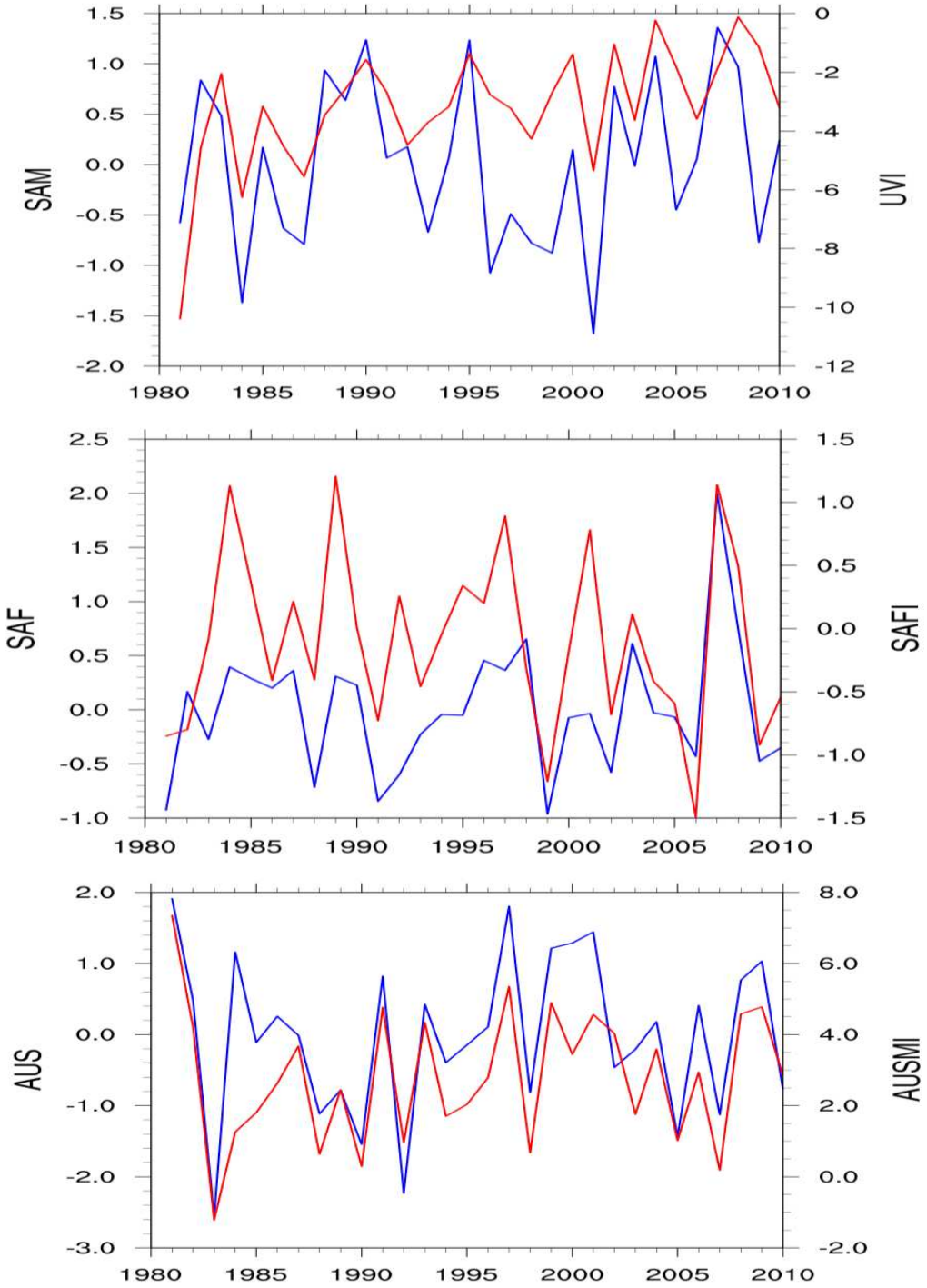

Figure 11 - Time Serie of the SMIs (red line) and SMRIs (blue line) for CFSR and GPCP data, 1981-2010 (DJF).

3.5 Interannual variability summer monsoon indices

In this section we intend to investigate the teleconnections between SMIs, and some dynamic characteristics of the monsoon related to these continents in SH that can influence each other. Through correlation fields between each SMIs

with precipitation, SLP and SST, with observed datasets and the CMIP5 models during the interval 1981 to 2010 relating to austral summer.

3.5.1. *UVI index*

Figure 12 shows the spatial pattern of correlation between DJF rainfall anomalies and UVI index by GPCP datasets and CMIP5 models. The GPCP display positive correlations over northwest-southern region embedded in the South Atlantic Convergence Zone (SACZ). On the other hand, rainfall below average is observed over the southern SA and adjacent Pacific Ocean (negative correlation). This shows that the UVI index displays a dipole pattern of precipitation anomaly over SA, in addition, a reduced precipitation over Australia and positive anomalies of rainfall over the western coast of Africa, in the Indian Ocean and over Madagascar. In general, most CMIP5 models reproduce the GPCP pattern, though they deliver positive anomalies on Southern Africa and Australia, differ from that observed by GPCP dataset. Nevertheless, the CFSv2-2011 does not show significant correlation with any domain monsoon.

Positive (negative) precipitation anomaly observed on SA is associated with low (high) pressure (Figure 13). Under positive anomalies of SLP, the transport of warm and moist air over monsoon is increased, contributing to the convective instability in monsoon domains. The CMIP5 models differ in the spatial pattern of correlation over northeast and southeast in SA and Atlantic Ocean. Overall they are able to reproduce the GPCP correlation map. The BCC-CSM1.1, GFDL-CM2.1, MIROC5, and MPI-ESM-LR models show negative pressure anomalies with the UVI index on the African continent, also associated with positive precipitation anomalies.

The pattern of correlation between UVI and SST shows positive anomalies over the Atlantic Ocean on the southern coast of SA, western Africa, Indian Ocean in the vicinity of the western coast of Australia and northern Indonesia (Figure 14 - HadISST). It is interesting to note that the models show a significant meridional thermal contrast on the southern coast of South America, especially in the IPSL-CM5A-LR, MIROC5 and MRI-CGCM3 models. Similar result was found by Veiga et al. (2002) during the spring season (SON),

suggesting that the monsoon rainfall can be modulated by this pattern of positive (south) and negative (north) correlations in the Brazilian coast.

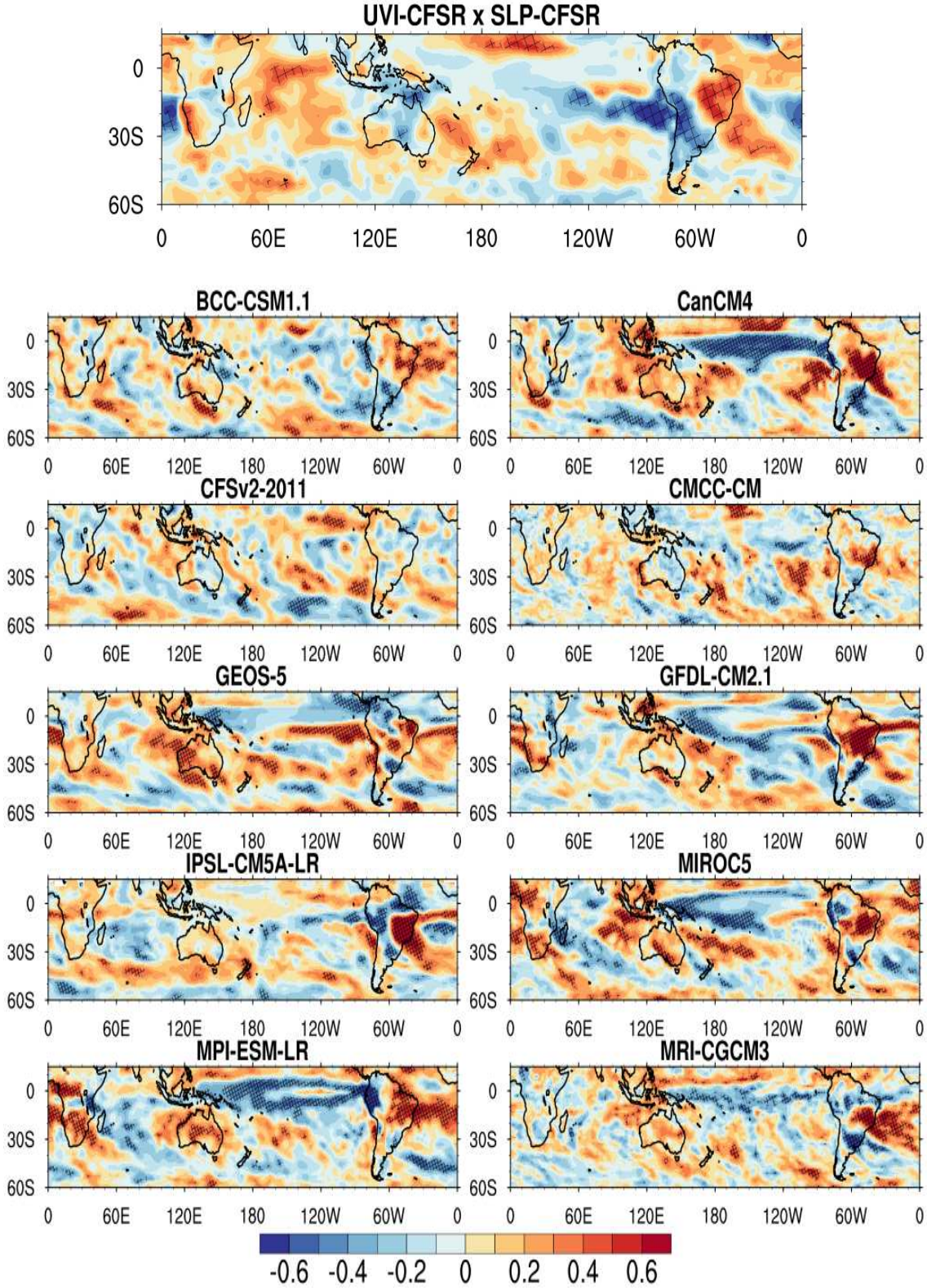

Figure 12 - Correlation coefficients between the DJF mean UVI and DFJ mean CFSR/GPCP and CMIP5 rainfall anomalies at each grid. Black grids represent correlations significant at 95% confidence.

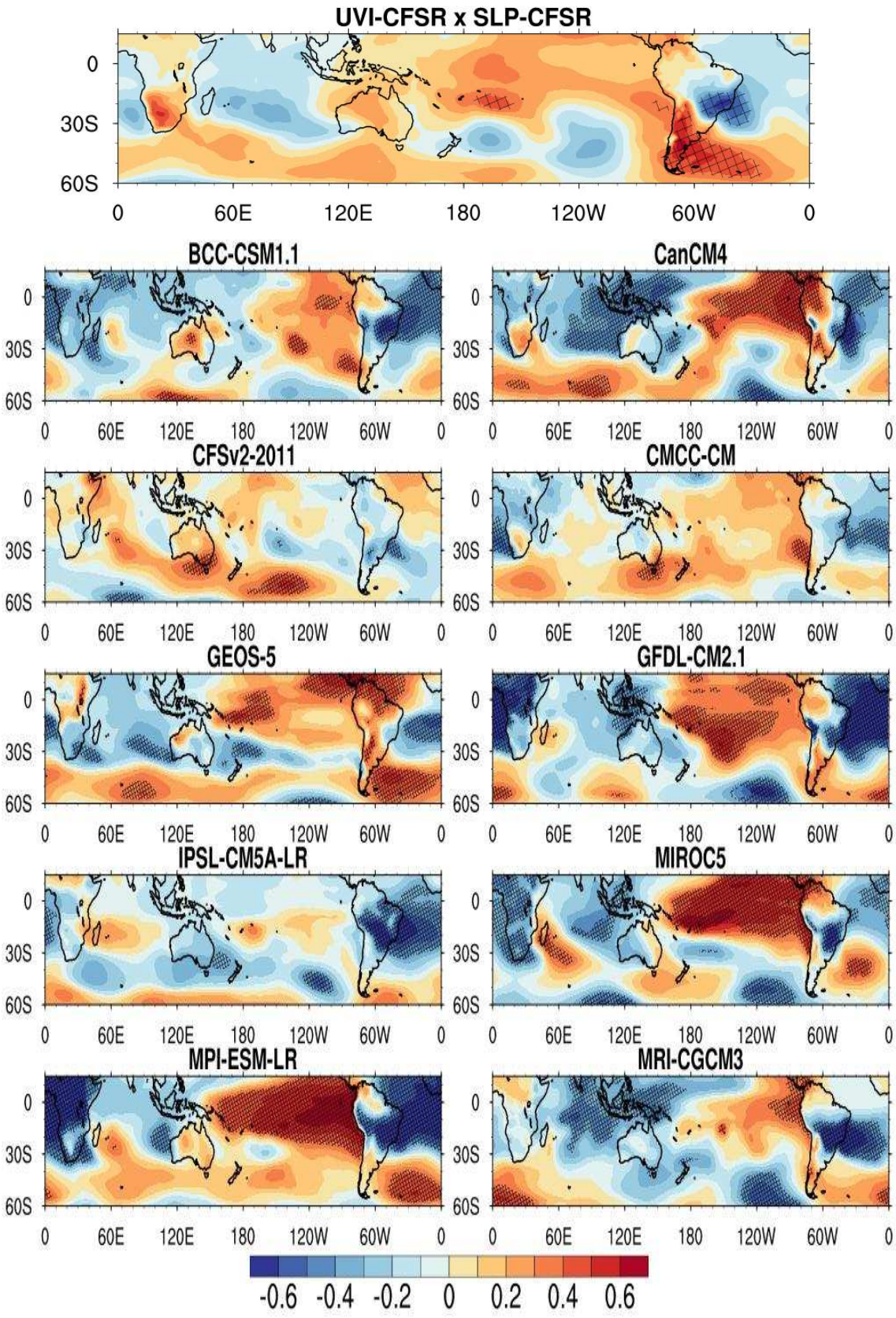

Figure 13 - The same in Figure 10 except for surface level pressure.

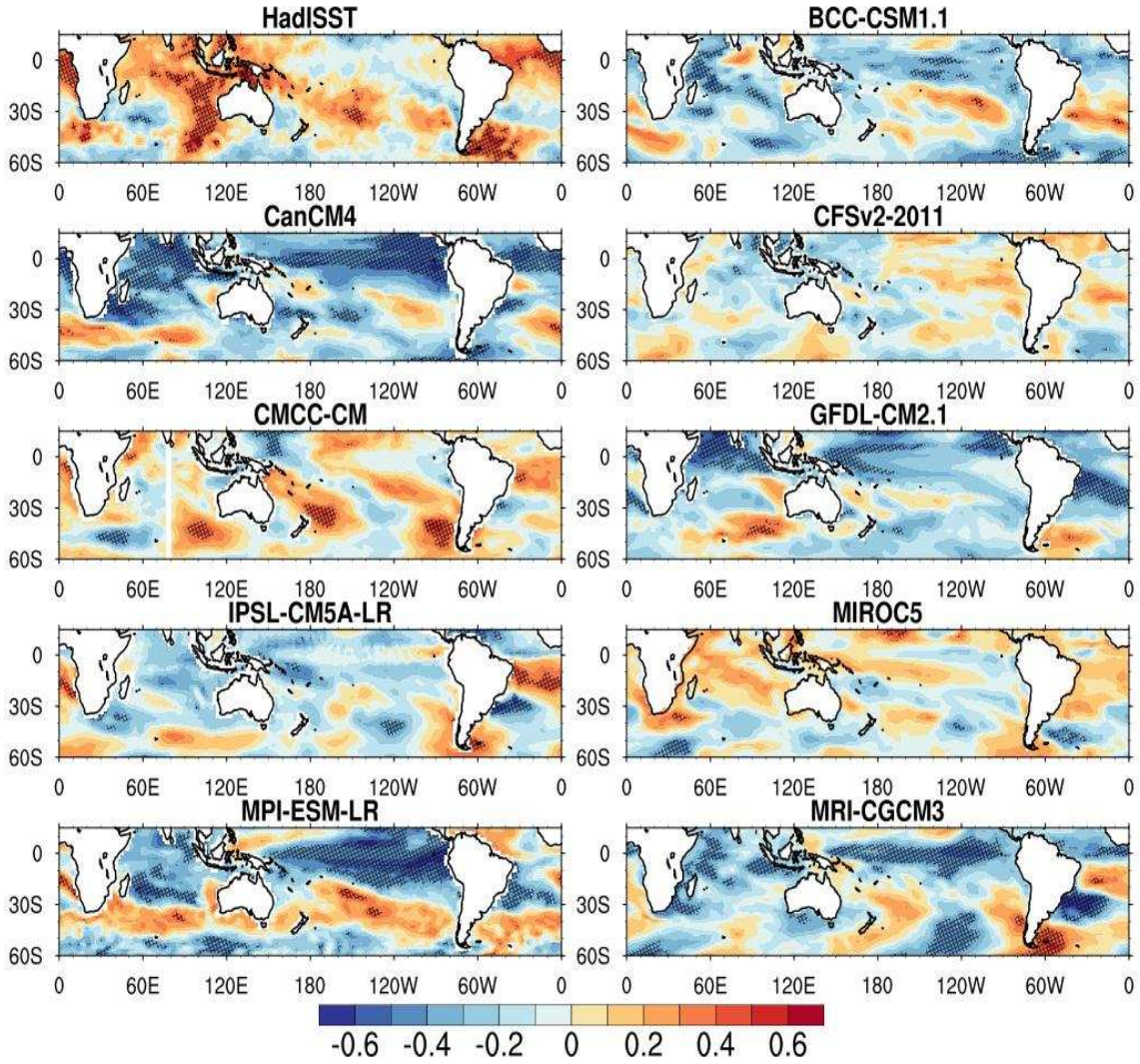

Figure 14 - The same in Figure 10 except for SST (ºC) (lack of GEOS-5 data).

3.5.2 *SAFI index*

In the following is investigated the African monsoon index and its association with the precipitation pattern. Correlation coefficients between SAFI and precipitation are shown in Figure 15. Positive correlation between SAFI and precipitation over the SAF domain are noticed, mainly in the Indian Ocean by GPCP dataset. For CMIP5 models, the CFSv2-2011 and CMCC-CM deliver very low correlation values. It should be noted that some models such as GEOS-5 and IPSL-CM5A-LR show higher correlation over other regions e.g. eastern SA and equatorial Pacific (negative correlation). The response is not that clear, however in Australia in the sense that positive and negative correlations are shown.

Changes to evaluation of the SLP (Figure 16) demonstrated a zonal dipole over the tropics/subtropics, but the magnitude is model dependent. A dominant feature is observed in the Indian Ocean where all models, except CFSv2-2011 depict negative correlation. The monsoonal region has no significant correlation with SST. The SAFI shows negative correlation only on east-equatorial Indian Ocean, east of Australia and subtropical Atlantic (Figure 17) .The SAFI as an indicator of the presence of monsoonal features is less representative than the climate response to the South America index- UVI, in relation the teleconnections with other monsoon domains.

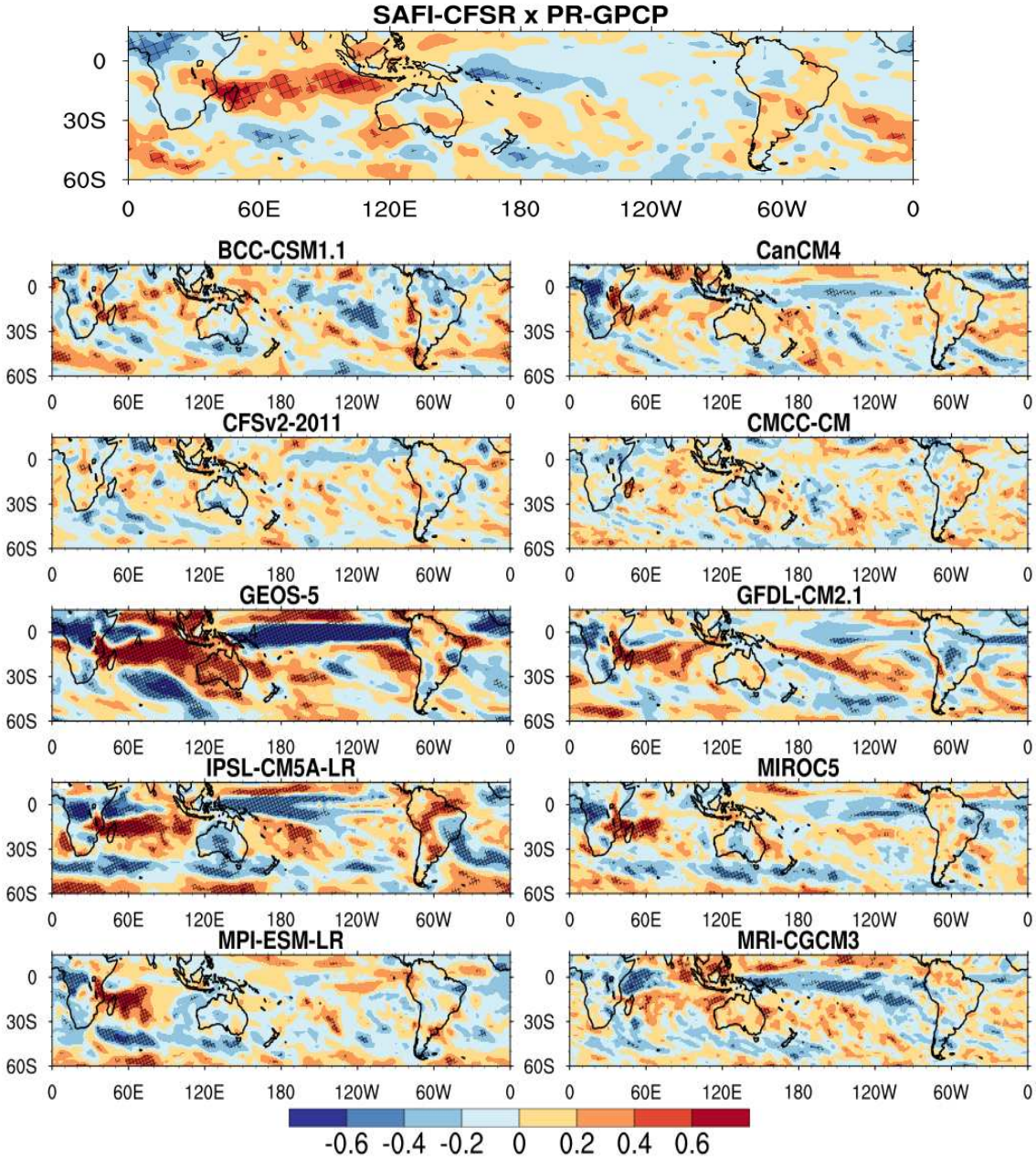

Figure 15- The same as Figure 10 except for SAFI index.

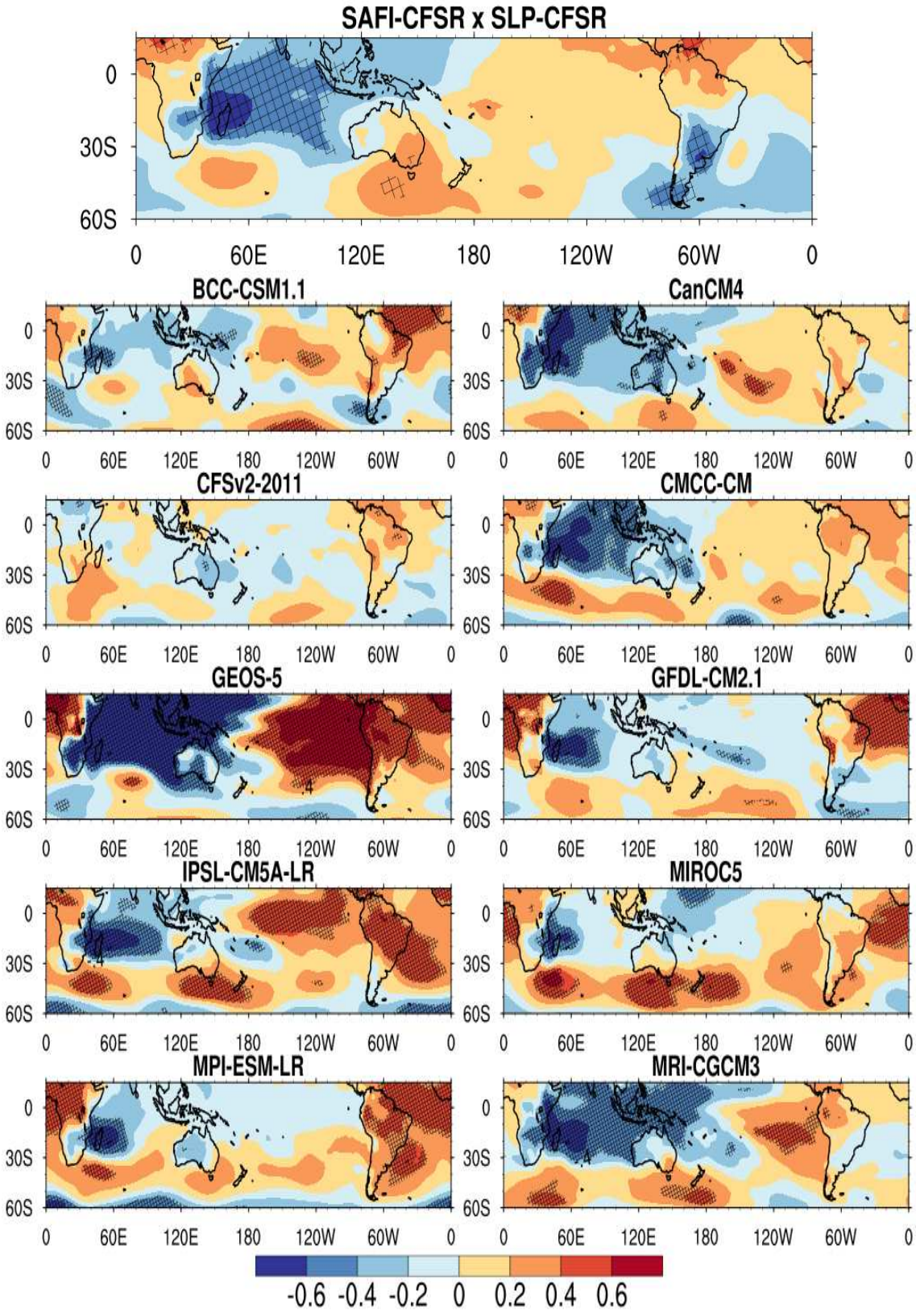

Figure 16- The same as Figure 10 except for sea level pressure, SAFI index.

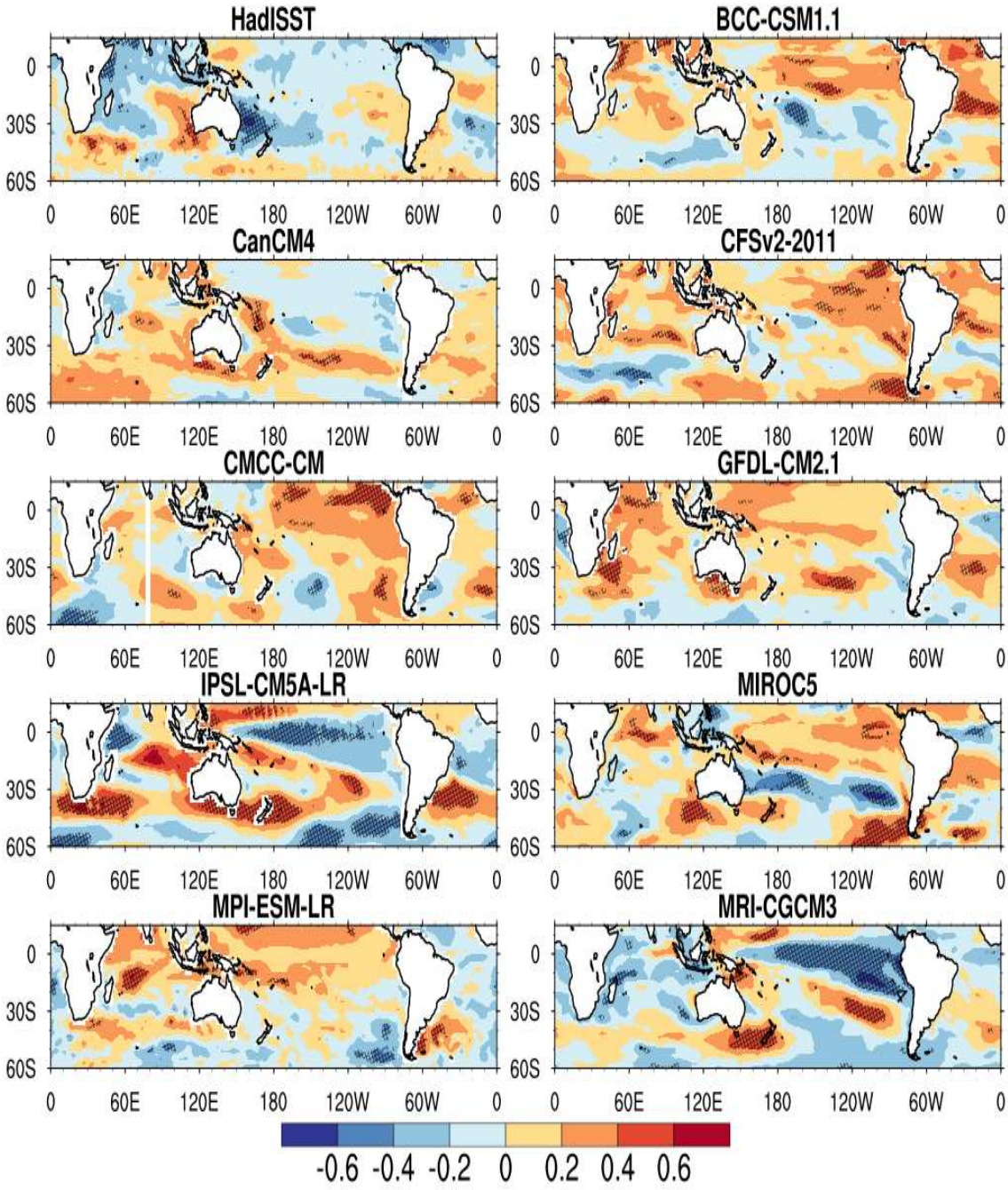

Figure 17- The same as Figure 10 except for SST to SAFI index.

3.5.3 *AUSMI index*

Figure 18 shows positive correlation between the AUSMI and precipitation over Australia/Indonesia domain for GPCP and CMIP5 models, as found by the definition of the index (Kajikawa et al. 2009). An interesting feature noticed in GPCP is the positive correlation also over southern Africa and northern SA. Negative correlations are found in the equatorial Pacific and the Indian Ocean.

This may indicate the potential of this index for predicting the monsoon system in SA and Africa. The models are able to reasonable reproduce the correlation pattern delivered by GPCP. Higher correlations are seen in CanCM4, GEOS-5, GFDL-CM2.1 and MIROC5. The GFDL-CM2.1 and MIROC5 also show positive correlation over the SAF domain.

For SLP (Figure 19) the seesaw effect is reproduced in the correlation pattern, with positive values over SA. Kullgren and Kim (2006) has demonstrated that prior to the monsoon onset, surface temperature increase, and SLP decrease over Australia, initiating an anomalous cyclonic circulation increasing low level moisture convergence and precipitation over northern Australia, as reproduced by circulation indice-AUSMI.

Significant negative correlation between AUSMI and SST (HadISST) is seen in the northern and eastern equatorial Indian Ocean and positive correlation over the western Pacific Ocean (Figure 20). This indicates that changes of winds at lower levels favor warm SST anomalies in the equatorial western Pacific, that associated with the lower SLP contribute to increase the warm and moist air advection over Australia and Indonesia, initiating a strong summer monsoon. This similar pattern is discussed in Kullgren and Kim (2006) and (Wu 2015). On the other hand, the strengthening of the summer monsoon over Australia is associated with negative anomaly of SST over the equatorial eastern Pacific. Only the MRI-CGCM3 reproduce the same spatial correlation pattern compared to the HadISST, but with smaller correlations.

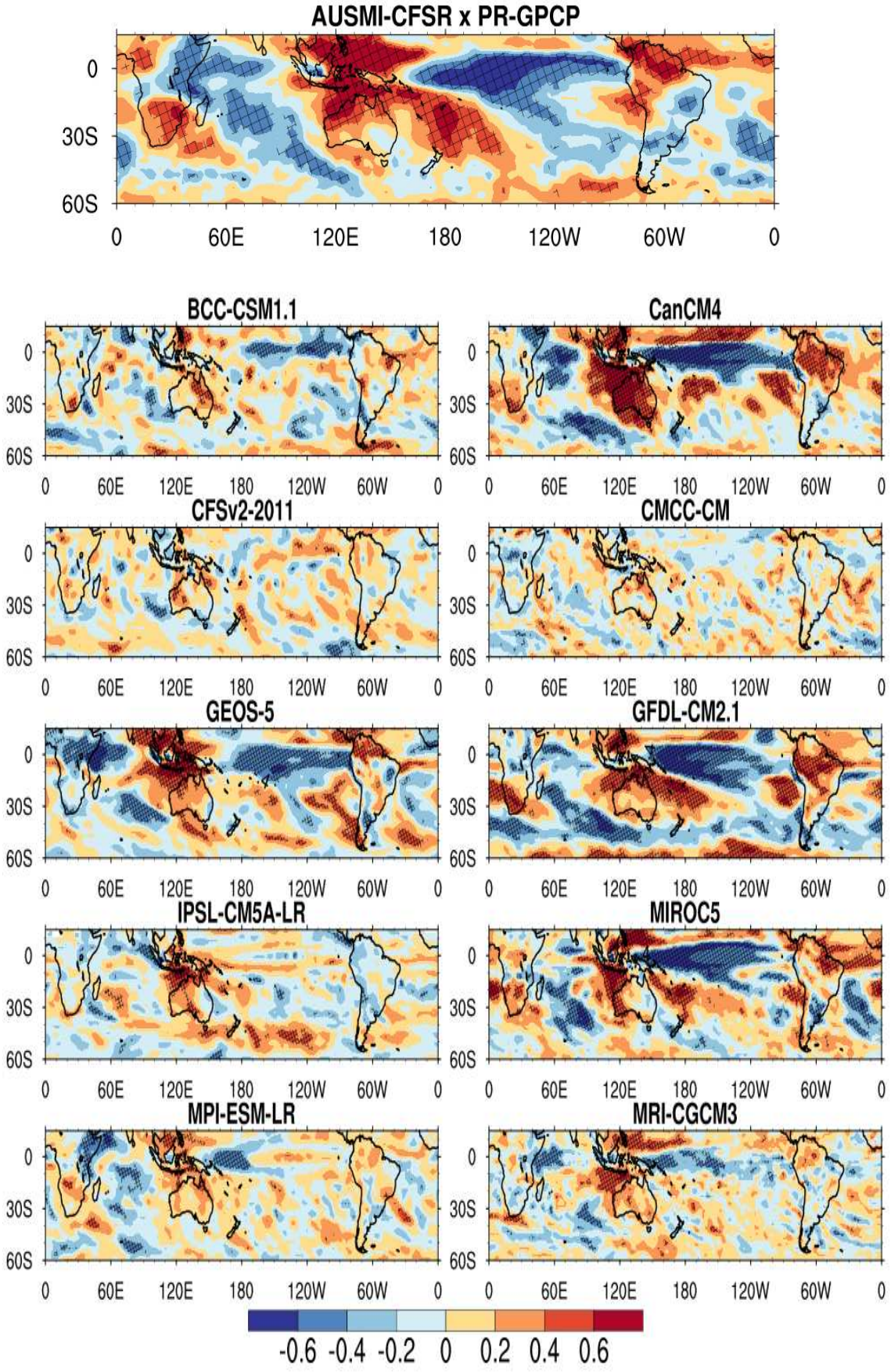

Figure 18- The same as Figure 10 except to AUSMI for precipitation (mm/day).

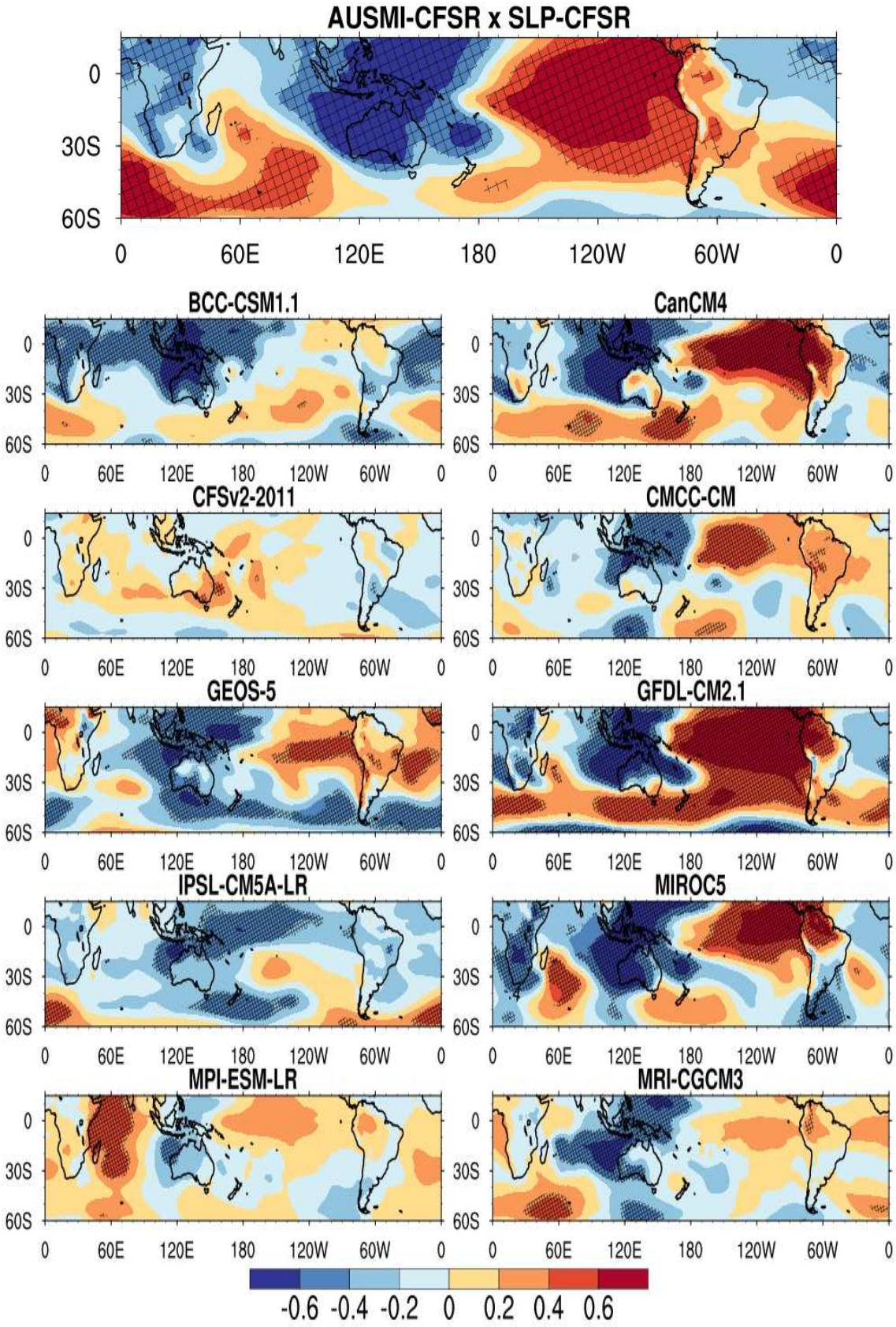

Figure 19- The same as Figure 10 except to AUSMI for sea level pressure.

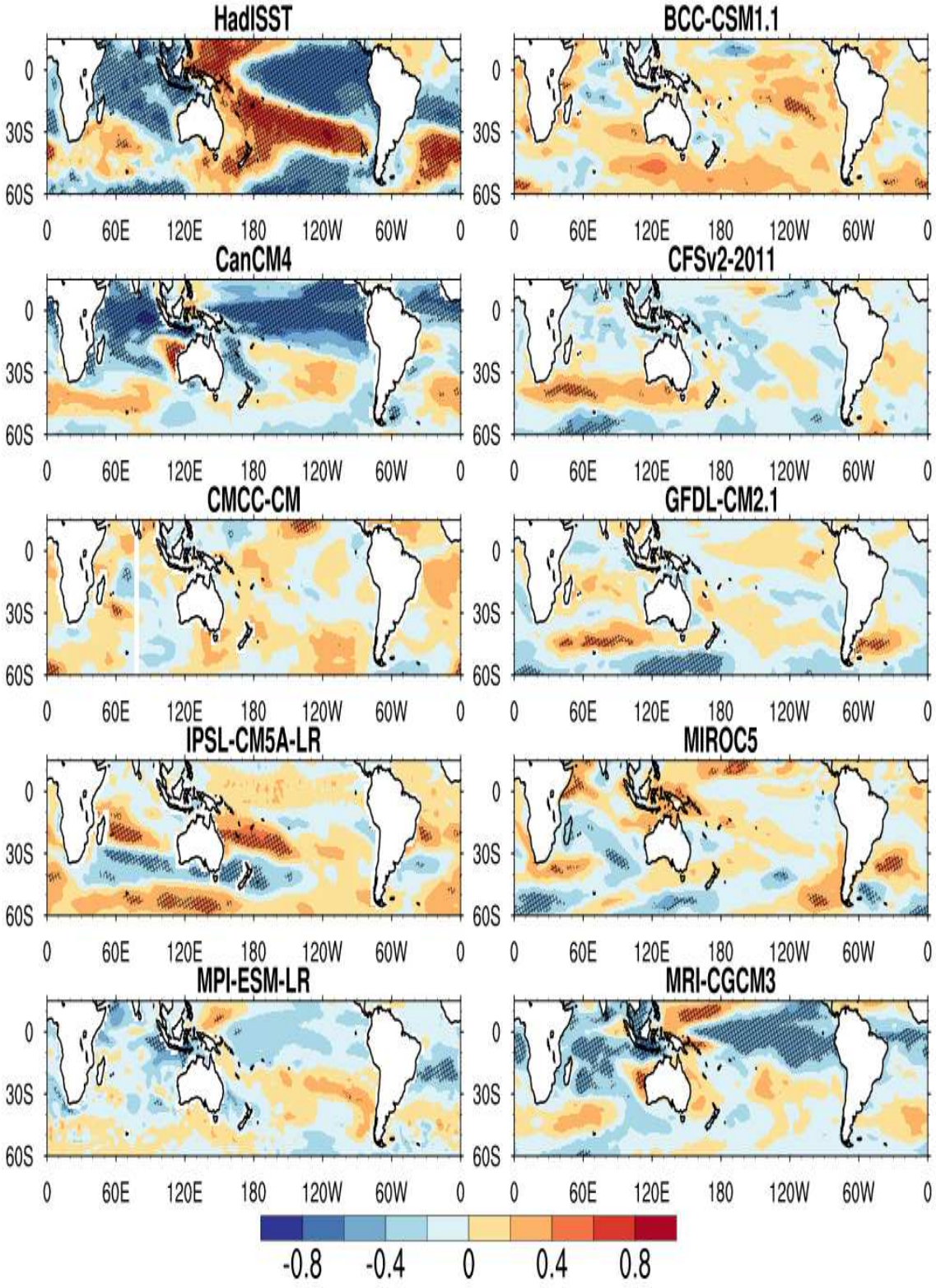

Figure 20 - The same as Figure 10 except to AUSMI for sea surface temperature (ºC) (lack of GEOS-5 data).

3.6 Influence of the Antarctic Oscillation in the summer monsoon rainfall

In this section, we investigated the influence of teleconnection of the AAO with the rainfall monsoon (austral summer) through the technique of composites, computing DJF mean refers AAO, because this is associated with the wet monsoon in SH.

The spatial influence of the AAO in the austral summer monsoon rainfall is analyzed in Figure 21 by GPCP and CMIP5 models. Most of the models are able to well reproduce the pattern observed with the reanalysis, in particular models CanCM4, CMCC-Cm and CFSv2-2011. The composite of the AAO with austral summer precipitation in SH, shows that the strongest connection occurs on the Pacific Ocean, near Australia and Indonesia.

Positive precipitation anomalies are observed in a southeast, over the climatological position of the SACZ in South America. Some models confirm the positive signal to the SACZ, such as MIROC5 and BCC-CSM1.1, for the IPSL-CM5A-LR and GEOS-5 showing the opposite response. This result agrees with analyses by Carvalho et al. (2005) and Reboita et al. (2009). Negative (positive) anomalies are also observed over southern (northern) South America. Negative anomalies may be noted in the equatorial region, in particular in CMCC-CM, GEOS-5, GFDL-CM2.1, MIROC5 and MPI-ESM-LR. In Southern Africa the models in large part agree with the pattern observed by GPCP data. Positive anomalies (negative) over the southern region (north of 15ºS) associated with positive (negative) phase of the AAO. In the Australian continent positive anomalies are dominate in most models. The GFDL-CM2.1 overestimates the anomalies, while the IPSL-CM5A-LR has practically no anomalies associated with AAO.

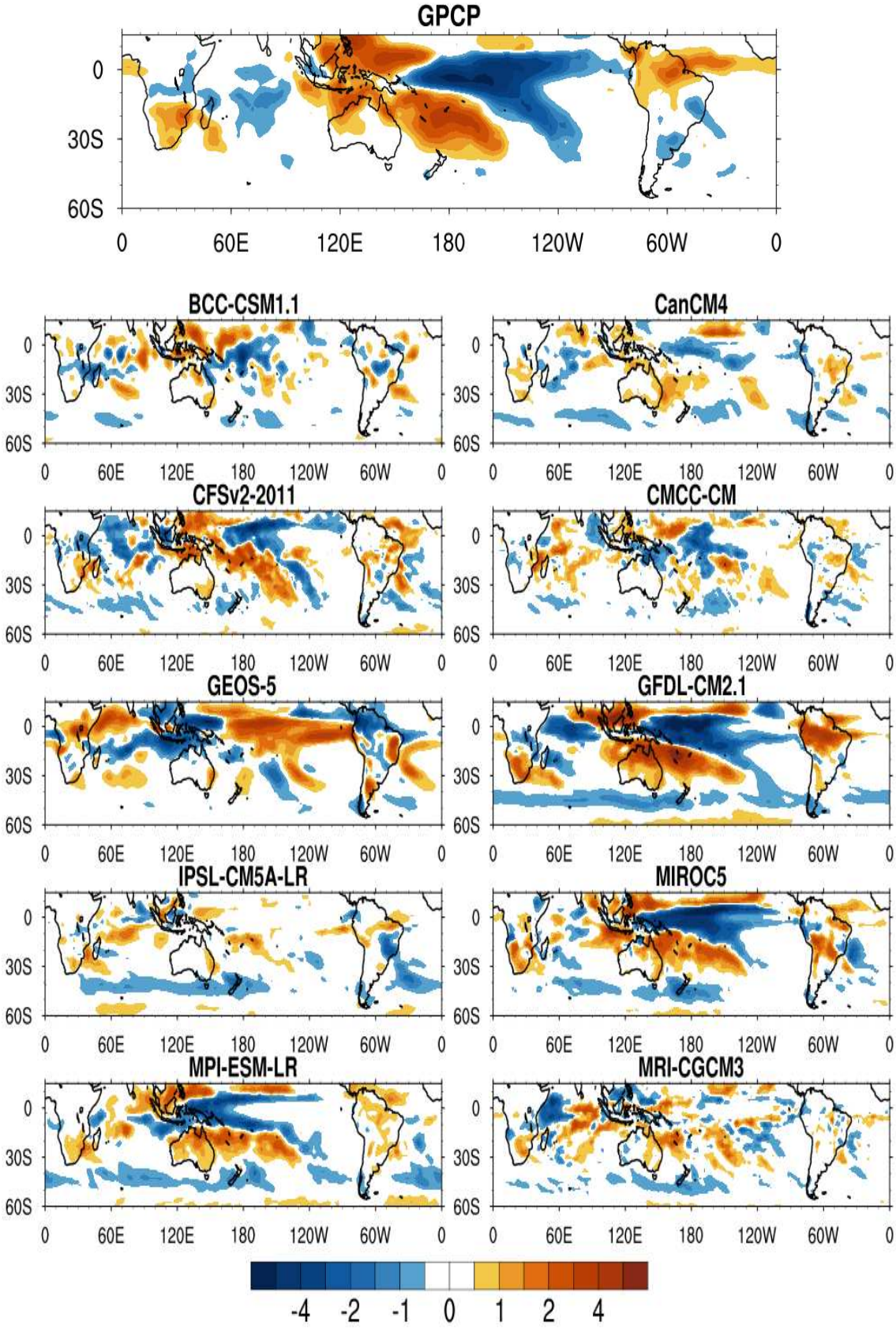

Figure 21 - Difference between the positive composite and negative composite of the AAO in precipitation (mm/day) in DJF.

3.7 Relationship of the El Niño Southern Oscillation

As is well known, the summer monsoon rainfall is associated with intensity ENSO phases for the SH domains monsoon. The SAM is related with SST dipole in the southwest Atlantic Ocean, while, AUS is associated with a mature state of La Niña events, as seen in Figures 14 and 20, according to previous studies. The SAF has no significant correlations with ENSO (SST). In addition, we examine how the SMIs and AAO are related to ENSO, computed as Niño3.4 index (5ºS-5ºN, 170ºW-120ºW) by HadISST dataset, in DJF mean associated mature stage of the ENSO phases.

The behavior of SMIs in relation to the interannual variability of the AAO and ENSO are shows by normalized time serie in Figure 22. It is clear that negative peak observed in 1983 is closely linked to phases of the AAO and ENSO. Moreover, the AAO indice is inversely proportional to the ENSO phases, with negative (positive) AAO phase linked with years of El Niño (La Niña), as pointed by other studies. On the other hand, the relationship circulation indices with phases ENSO and AAO differ from each other. In El Niño years, for example 1983 and 1998 the UVI follows in the same phase of NINO3.4 and the AAO, respectively. The SAFI is linked to NINO3.4 while AUSMI with the AAO. In La Niña years (e.g. 1989 and 2008), it is observed that the three indices are associated in phase with the AAO.

Furthermore, correlation coefficient between AAO-ENSO and SMIs-SMIRs are more significant for Australia compared to other domains of the SH (Table 3). However, the CMIP5 models show a strong correlation also between SMIRs-SMIs and the ENSO. The CanCM4 and CFSv2-2011 models are strongly correlated with the ENSO, whereas, the IPSL-CM5A-LR and MIROC5 with the AAO, with respect SMIs and SMIRs, respectively. In general, it is noted that the variability of teleconnections are best correlated with rainfall indices in relation to circulation indices for ENSO.

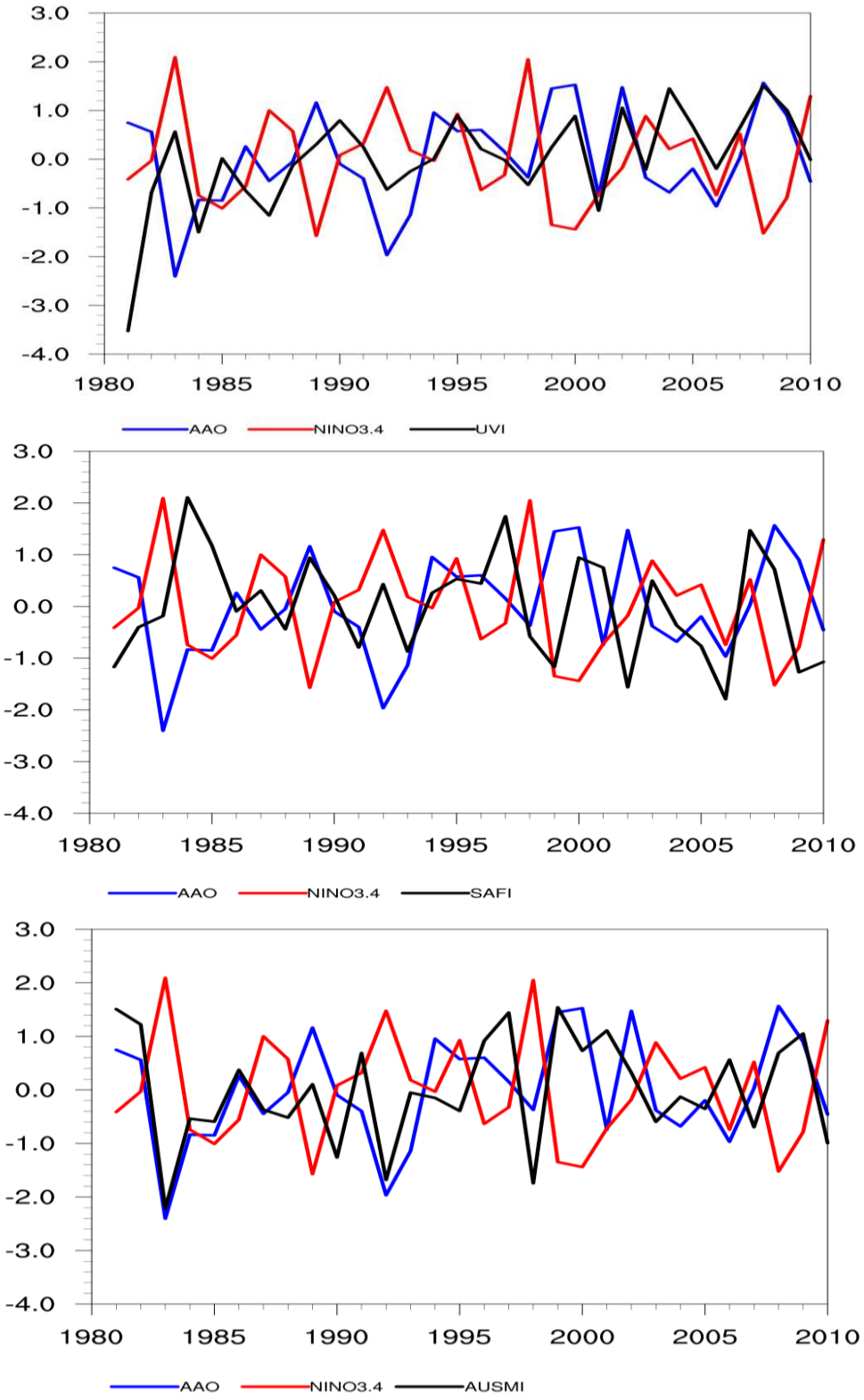

Figure 22 - Time series normalized DJF seasonal mean of the Antarctic Oscillation (blue line), NINO3.4 (red line), and SMIs (black line) from CFSR/GPCP.

Table 3- The correlation coefficients between the AAO/ENSO (DJF) and summer monsoon indices and rainfall summer monsoon indices in the rectangular domains.

Observed/ Models	Monsoon Domains	CC AAO x SMIs	CC AAO x SMIRs	CC NINO3.4 x SMIs	CC NINO3.4 x SMIRs
GPCP/HadISST	SAM	0.21	0.12	-0.070	0.16
	SAF	-0.047	0.047	-0.16	0.04
	AUS	**0.45***	**0.43***	**-0.51***	**0.014***
BCC-CSM1.1	SAM	-0.009	**0.43***	**-0.34***	0.064
	SAF	-0.19	-0.29	0.28	**0.33****
	AUS	0.21	0.23	**0.30****	0.17
CanCM4	SAM	0.24	0.28	**-0.50***	**-0.56***
	SAF	-0.045	0.16	-0.16	**0.46***
	AUS	-0.34	-0.15	**-0.52***	**-0.73***
CFSv2-2011	SAM	0.25	0.12	**-0.39***	**0.35***
	SAF	0.035	-0.081	**0.35***	0.20
	AUS	**-0.40***	-0.22	**-0.56***	**-0.71***
CMCC	SAM	0.13	0.25	0.030	**0.31****
	SAF	0.084	**0.36***	0.28	**-0.47***
	AUS	-0.11	-0.17	0.14	0.15
GEOS-5	SAM	**-0.33****	-0.17	-	-
	SAF	-0.24	-0.18	-	-
	AUS	-0.28	**-0.47***	-	-
GFDL-CM2.1	SAM	0.043	0.24	-0.28	0.29
	SAF	-0.028	0.21	0.12	0.22
	AUS	**-0.63***	**-0.55***	0.07	-0.025
IPSL-CM5A-LR	SAM	-0.25	-0.27	-0.09	-0.16
	SAF	**0.32****	0.11	**-0.41***	0.24
	AUS	**-0.20***	-0.009	-0.003	0.031
MIROC5	SAM	0.25	**0.35***	-0.08	-0.15
	SAF	**-0.39***	-0.054	0.21	0.26
	AUS	-0.34	**-0.35***	0.023	-0.048
MPI-ESM-LR	SAM	0.21	0.20	**-0.50***	**-0.39***
	SAF	**-0.37***	-0.15	0.15	**0.33****
	AUS	-0.14	0.010	**-0.30****	-0.23
MRI-CGCM3	SAM	-0.08	0.014	**-0.46***	**-0.32****
	SAF	-0.21	-0.030	**-0.53***	0.038
	AUS	-0.026	-0.09	0.29	0.26

The bolder numbers with "*" and "**" symbols represent statistical significant at 95% and 90%, respective confidence level (lack GEOS-5 data).

4. Conclusions

This paper evaluated ten models simulation that support the IPCC AR5, to assess the state-of-the-art reproducing the interannual variability of the summer monsoon over SH domains.

Simulated precipitation, surface temperature and winds were compared with reanalysis CFSR and reconstructed GPCP datasets. It has been demonstrated that some models presented several differences compared with observational

datasets and reanalysis. The CFSv2-2011 and BCC-CSM1.1 models show the largest temperature bias over Antarctic continent, up to – 20/10 K as compared to CFSR. The GEOS-5 exhibits a cold bias over Antarctic. The CanCM4 model shows a very reasonable temperature pattern. All models overestimate precipitation in the tropics, solely CanCM4 follows the observed pattern but underestimates rainfall in this region. Based on harmonic analyses it has been found that the models are able to simulate the seasonal cycle of rainfall. Positive anomalies of precipitation are linked with variability of the zonal wind at surface, especially on regions under the influence of the monsoon regime. It is also observed that the models exhibit lower contrasts precipitation and temperature in relation to the observed datasets, to reproduce relatively well the simulations compared with observed.

Overall models feature large uncertainties in simulating climate variability in SH, since some models simulate very well some variables while the other variables are uncertain. This study explored only the differences between the CMIP5 simulations with observed datasets. However, further investigation is required on the uncertainties and biases associated with climate models.

Investigations between the monsoon indices in the SH shows that the rains in monsoon domains are commonly characterized with low pressure anomalies associated with low-level cyclonic circulation and SST gradient. The association between UVI and AUSMI show a dipole low (high) pressure over South America and Australia, this contributes to seesaw effect of precipitation, with positive (negative) anomaly between SAM (AUS). The AUSMI index plays role in the rains in the SAF domain, reporting positive (negative) anomaly rainfall over region southern Madagascar and west (northern Madagascar and northeastern). UVI index displays a dipole pattern of precipitation anomalies over South America associated with increased (decrease) rainfall over northeast-southeast Brazil (southern-west central of South America), strongly linked with high (low) anomalies pressure.

AAO's relationship with austral summer precipitation in SH shows significant correlation with AUS domain, this is related to the strongest connection that occurs on the Pacific Ocean, near Australia and Indonesia. The CMIP5 models show a strong correlation also between the ENSO phases and SMIs-SMIRs, mainly CanCM4 and CFSv2-2011 models.

The circulation indices analyzed in this study proved useful to monitor the impact of variability of summer monsoon rainfall regionally and on a large scale. These indices can also be helpful in the assessment of the CMIP5 models in simulating the future changes in regional monsoons. It should be noted that our study did not evaluate the summer monsoon indices in climatic change scenarios, as well as compare differences associated with CMIP5 models depending on the magnitude of the forcing of greenhouse gases, that will be calls for further study. It is important, moreover, to investigate the vertical structure of the atmosphere to figure out the propagation of teleconnection patterns among monsoon regions, based on time lag correlations and to include analysis of latent and sensible heat fluxes.

Acknowledgments. This work was supported by Brazilian National Council for Scientific and Technological Development – CNPq. The authors acknowledge the World Climate Research Programme's Working Group on Coupled Modelling, which is responsible for CMIP, and the climate modeling. The authors also acknowledge the insightful comments from two anonymous reviewers, which helped to improve this paper.

REFERENCES

Adler, R. F., and Coauthors, 2003: The Version-2 Global Precipitation Climatology Project (GPCP) Monthly Precipitation Analysis (1979–Present). *J. Hydrometeorol.*, **4**, 1147–1167, doi:10.1175/1525-7541(2003)004<1147:TVGPCP>2.0.CO;2.

Asnani, G. C. Tropical meteorology. Pune, Índia: Nobel Printers, 1993.

Campos, T. L. O. B., 2013: Influência dos padrões de variabilidade de baixa frequência na precipitação da amazônia. *Diss. Mestr.*,.

Carvalho, L. M. V, C. Jones, and T. Ambrizzi, 2005: Opposite phases of the Antarctic oscillation and relationships with intraseasonal to interannual activity in the tropics during the austral summer. *J. Clim.*, **18**, 702–718, doi:10.1175/JCLI-3284.1.

Chylek, P., J. Li, M. K. Dubey, M. Wang, and G. Lesins, 2011: Observed and model simulated 20th century Arctic temperature variability: Canadian

Earth System Model CanESM2. *Atmos. Chem. Phys. Discuss.*, **11**, 22893–22907, doi:10.5194/acpd-11-22893-2011.

Delworth, T. L., and Coauthors, 2006: GFDL's CM2 global coupled climate models. Part I: Formulation and simulation characteristics. *J. Clim.*, **19**, 643–674, doi:10.1175/JCLI3629.1.

Dufresne, J. L., and Coauthors, 2013: Climate change projections using the IPSL-CM5 Earth System Model: from CMIP3 to CMIP5. *Climate Dynamics*.

Endo, H., and A. Kitoh, 2014: Thermodynamic and dynamic effects on regional monsoon rainfall changes in a warmer climate. *Geophys. Res. Lett.*, **41**, 1704–1710, doi:10.1002/2013GL059158.

Gan, M. a., V. E. Kousky, and C. F. Ropelewski, 2004: The South America Monsoon circulation and its relationship to rainfall over west-central Brazil. *J. Clim.*, **17**, 47–66, doi:10.1175/1520-0442(2004)017<0047:TSAMCA>2.0.CO;2.

Gan, M. A., V. B. Rao, and M. C. L. Moscati, 2006: South American monsoon indices. *Atmos. Sci. Lett.*, **223**, 219–223, doi:l0.l00Zasl'l l9 South.

Gong, D., and S. Wang, 1999: Definition of Antarctic Oscillation index. *Geophys. Res. Lett.*, **26**, 459, doi:10.1029/1999GL900003.

Hendon, H. H., and B. Liebmann, 1990: A composite study of onset of the Australian summer monsoon. doi:10.1175/1520-0469(1990)047<2227:ACSOOO>2.0.CO;2.

Hirota, N., and Y. N. Takayabu, 2013: Reproducibility of precipitation distribution over the tropical oceans in CMIP5 multi-climate models compared to CMIP3. *Clim. Dyn.*, **41**, 2909–2920, doi:10.1007/s00382-013-1839-0.

Jakubauskas, M. E., D. R. Legates, and J. H. Kastens, 2001: Harmonic analysis of time - series AVHRR NDVI data. *Photogramm. Eng. Remote sensinghotogrammetric Eng. Remote Sens.*, **67**, 461–470.

Justino, F., and W. R. Peltier, 2008: Climate anomalies induced by the Arctic and Antarctic Oscillations: Glacial Maximum and present-day perspective. *J. Clim.*, **21**, 459–475, doi:10.1175/2007JCLI1703.1.

——, A. Setzer, T. J. Bracegirdle, D. Mendes, A. Grimm, G. Dechiche, and C. E. G. R. Schaefer, 2011: Harmonic analysis of climatological temperature over Antarctica: Present day and greenhouse warming perspectives. *Int. J. Climatol.*, **31**, 514–530, doi:10.1002/joc.2090.

Kajikawa, Y., B. Wanga, and J. Yang, 2009: A multi-time scale Australian monsoon index. *Int. J. Climatol.*, **1**, doi:10.1002/joc.

Kitoh, A., H. Endo, K. Krishna Kumar, I. F. a Cavalcanti, P. Goswami, and T. Zhou, 2013: Monsoons in a changing world: A regional perspective in a global context. *J. Geophys. Res. Atmos.*, **118**, 3053–3065, doi:10.1002/jgrd.50258.

Kullgren, K., and K. Y. Kim, 2006: Physical mechanisms of the Australian summer monsoon: 1. Seasonal cycle. *J. Geophys. Res. Atmos.*, **111**, 1–13, doi:10.1029/2005JD006807.

Lee, J. Y., and B. Wang, 2014: Future change of global monsoon in the CMIP5. *Clim. Dyn.*, **42**, 101–119, doi:10.1007/s00382-012-1564-0.

Liu, J., B. Wang, S. Y. Yim, J. Y. Lee, J. G. Jhun, and K. J. Ha, 2012: What drives the global summer monsoon over the past millennium? *Clim. Dyn.*, **39**, 1063–1072, doi:10.1007/s00382-012-1360-x.

Nieto-Ferreira, R., and T. M. Rickenbach, 2011: Regionality of monsoon onset in South America: A three-stage conceptual model. *Int. J. Climatol.*, **31**, 1309–1321, doi:10.1002/joc.2161.

Parth Sarthi, P., S. Ghosh, and P. Kumar, 2015: Possible future projection of Indian Summer Monsoon Rainfall (ISMR) with the evaluation of model performance in Coupled Model Inter-comparison Project Phase 5 (CMIP5). *Glob. Planet. Change*, **129**, 92–106, doi:10.1016/j.gloplacha.2015.03.005.

Raddatz, T. J., and Coauthors, 2007: Will the tropical land biosphere dominate the climate-carbon cycle feedback during the twenty-first century? *Clim. Dyn.*, **29**, 565–574, doi:10.1007/s00382-007-0247-8.

Rayner, N. A., D. E. Parker, E. B. Horton, C. K. Folland, L. V. Alexander, D. P. Rowell, E. C. Kent, and A. Kaplan, 2003: Global analyses of sea surface temperature, sea ice, and night marine air temperature since the late Nineteenth Century. *J. Geophys. Res.*, **108**, doi:10.1029/2002JD002670.

Reboita, M. S., T. Ambrizzi, and R. P. Da Rocha, 2009: Relationship between the southern annular mode and southern hemisphere atmospheric systems. *Rev. Bras. Meteorol.*, **24**, 48–55, doi:10.1590/S0102-77862009000100005.

Reynolds, R. W., and T. M. Smith, 1995: A High-Resolution Global Sea Surface Temperature Climatology. *J. Clim.*, **8**, 1571–1583, doi:10.1175/1520-0442(1995)008<1571:AHRGSS>2.0.CO;2. http://journals.ametsoc.org/doi/abs/10.1175/1520-0442(1995)008<1571:AHRGSS>2.0.CO;2\nhttp://journals.ametsoc.org/doi/abs/10.1175/1520-0442(1995)008<1571:AHRGSS>2.0.CO;2.

Richter, I., S. P. Xie, A. T. Wittenberg, and Y. Masumoto, 2012: Tropical Atlantic biases and their relation to surface wind stress and terrestrial precipitation. *Clim. Dyn.*, **38**, 985–1001, doi:10.1007/s00382-011-1038-9.

Rienecker, M., and Coauthors, 2008: The GEOS-5 Data Assimilation System-Documentation of Versions 5.0. 1, 5.1. 0, and 5.2. 0. *Tech. Rep. Ser. Glob. Model. Data Assim.*, **27**.

Saha, S., and Coauthors, 2010: The NCEP climate forecast system reanalysis. *Bull. Am. Meteorol. Soc.*, **91**, 1015–1057, doi:10.1175/2010BAMS3001.1.

——, and Coauthors, 2013: The NCEP Climate Forecast System Version 2. *J. Clim.*, **2**, 1–61.

SANTOS, I. D. A., and N. J. D. N. FRANCO, 2011: Anomalias da precipitação no Sul do Brasil e as teleconexões. *XVII Congr. Bras. Agrometeorol.*,.

Scoccimarro, E., and Coauthors, 2011: Effects of tropical cyclones on ocean heat transport in a high-resolution coupled general circulation model. *J. Clim.*, **24**, 4368–4384, doi:10.1175/2011JCLI4104.1.

Sharmila, S., S. Joseph, A. K. Sahai, S. Abhilash, and R. Chattopadhyay, 2015: Future projection of Indian summer monsoon variability under climate change scenario: An assessment from CMIP5 climate models. *Glob. Planet. Change*, **124**, 62–78, doi:10.1016/j.gloplacha.2014.11.004.

Sikka, D. R., and S. Gadgil, 1980: On the Maximum Cloud Zone and the ITCZ over Indian, Longitudes during the Southwest Monsoon. *Mon. Weather Rev.*, **108**, 1840–1853, doi:10.1175/1520-0493(1980)108<1840:OTMCZA>2.0.CO;2.

Silva, A. R., 2008: Ciclo de vida do sistema de monção da América do Sul: Observação e simulação. *Tese Doutorado*,.

Sperber, K. R., H. Annamalai, I. S. Kang, A. Kitoh, A. Moise, A. Turner, B. Wang, and T. Zhou, 2013: *The Asian summer monsoon: An intercomparison of CMIP5 vs. CMIP3 simulations of the late 20th century*. Climate Dynamics, 2711-2744 pp.

Srivastava, a K., M. Rajeevan, and S. R. Kshirsagar, 2009: Development of a high resolution daily gridded temperature data set (1969 – 2005) for the Indian region. *Atmos. Sci. Lett.*, **10**, 249–254, doi:10.1002/asl.

Tapiador, F. J., and Coauthors, 2012: Global precipitation measurement: Methods, datasets and applications. *Atmos. Res.*, **104-105**, 70–97, doi:10.1016/j.atmosres.2011.10.021. http://dx.doi.org/10.1016/j.atmosres.2011.10.021.

Taylor, K. E., R. J. Stouffer, and G. a Meehl, 2009: A Summary of the CMIP5 Experiment Design. **4**, 1–33, doi:10.1175/BAMS-D-11-00094.1. http://cmip-pcmdi.llnl.gov/cmip5/docs/Taylor_CMIP5_design.pdf.

Taylor, K. E., R. J. Stouffer, and G. a. Meehl, 2012a: An overview of CMIP5 and the experiment design. *Bull. Am. Meteorol. Soc.*, **93**, 485–498, doi:10.1175/BAMS-D-11-00094.1.

——, ——, and ——, 2012b: An overview of CMIP5 and the experiment design. *Bull. Am. Meteorol. Soc.*, **93**, 485–498, doi:10.1175/BAMS-D-11-00094.1.

Thompson, D. W. J., and J. M. Wallace, 2000: Annular Mode in the Extratropical Circulation. Part I : Month-to-Month Variability. *J. Clim.*, **13**, 1000–1016.

Trenberth, K. E., D. P. Stepaniak, and J. M. Caron, 2000: The global monsoon as seen through the divergent atmospheric circulation. *J. Clim.*, **13**, 3969–3993, doi:10.1175/1520-0442(2000)013<3969:TGMAST>2.0.CO;2.

Vasconcellos, F. C., and I. F. a Cavalcanti, 2010: Extreme precipitation over Southeastern Brazil in the austral summer and relations with the Southern Hemisphere annular mode. *Atmos. Sci. Lett.*, **11**, 21–26, doi:10.1002/asl.247.

Veiga, J. a. P., J. a. Marengo, and V. B. Rao, 2002: A influencia das anomalias de TSM dos oceanos Pacífico e Atlântico sobre as chuvas de monção da AS. *Rev. Bras. Meteorol.*, **17**, 181–194.

Wang, B., and Q. Ding, 2008: Global monsoon: Dominant mode of annual variation in the tropics. *Dyn. Atmos. Ocean.*, **44**, 165–183, doi:10.1016/j.dynatmoce.2007.05.002.

——, J. Liu, H. J. Kim, P. J. Webster, and S. Y. Yim, 2012: Recent change of the global monsoon precipitation (1979-2008). *Clim. Dyn.*, **39**, 1123–1135, doi:10.1007/s00382-011-1266-z.

——, S. Y. Yim, J. Y. Lee, J. Liu, and K. J. Ha, 2014: Future change of Asian-Australian monsoon under RCP 4.5 anthropogenic warming scenario. *Clim. Dyn.*, **42**, 83–100, doi:10.1007/s00382-013-1769-x.

Wang, P., 2009: Global monsoon in a geological perspective. *Chinese Sci. Bull.*, **54**.

Watanabe, M., and Coauthors, 2010: Improved climate simulation by MIROC5: Mean states, variability, and climate sensitivity. *J. Clim.*, **23**, 6312–6335, doi:10.1175/2010JCLI3679.1.

Webster, P. J., V. O. Magaña, T. N. Palmer, J. Shukla, R. A. Tomas, M. Yanai, and T. Yasunari, 1998: Monsoons: Processes, predictability, and the prospects for prediction. *J. Geophys. Res.*, **103**, doi:10.1029/97JC02719.

Wilks, D. S., 2006: *Statistical Methods in the Atmospheric Sciences*. 627 pp.

Wu, R., 2015: Possible roles of regional SST anomalies in long-term changes in the relationship between the Indian and Australian summer monsoon rainfall. *Theor. Appl. Climatol.*, doi:10.1007/s00704-015-1443-9. http://link.springer.com/10.1007/s00704-015-1443-9.

Xin, X.-G., T.-W. Wu, and J. Zhang, 2013: Introduction of CMIP5 Experiments Carried out with the Climate System Models of Beijing Climate Center. *Adv. Clim. Chang. Res.*, **4**, 41–49, doi:10.3724/SP.J.1248.2013.041.

Yim, S.-Y., B. Wang, J. Liu, and Z. Wu, 2013: A comparison of regional monsoon variability using monsoon indices. *Clim. Dyn.*, **43**, 1423–1437, doi:10.1007/s00382-013-1956-9.

Yue, S., P. Pilon, and G. Cavadias, 2002: Power of the Mann-Kendall and Spearman's rho tests for detecting monotonic trends in hydrological series. *J. Hydrol.*, **259**, 254–271, doi:10.1016/S0022-1694(01)00594-7.

Yukimoto, S., and Coauthors, 2011: Meteorological Research Institute-Earth System Model Version 1 (MRI-ESM1). *Tech. Reports*, **64**, 88.

Yulihastin, E., and E. Hermawan, 2012: Annual Migration of Monsoon Over Indonesia Maritime Continent Based on OLR Data. **35**, 27–39.

Zhang, S., and B. Wang, 2008: Global summer monsoon rainy seasons. *Int. J. Climatol.*, doi:10.1002/joc.1659 Global. http://www3.interscience.wiley.com/journal/4735/home.

Zhisheng, A., and Coauthors, 2014: Global Monsoon Dynamics and Climate Change. *Annu. Rev. Earth Planet. Sci.*, **43**, doi:10.1146/annurev-earth-060313-054623.

Zhou, J., and K. M. Lau, 1998: Does a monsoon climate exist over South America? *J. Clim.*, **11**, 1020–1040, doi:10.1175/1520-0442(1998)011<1020:DAMCEO>2.0.CO;2.